2003

High strain rate properties of polymer matrix composites

Amol Jadhav
Louisiana State University and Agricultural and Mechanical College

HIGH STRAIN RATE PROPERTIES OF POLYMER MATRIX COMPOSITES

A Thesis

Submitted to the Graduate Faculty of the
Louisiana State University and
Agricultural and Mechanical College
in partial fulfillment of the
requirements for the degree of
Master of Science in Engineering Science

in

The Interdepartmental Program in Engineering Science

by
Amol Jadhav
B. S., University of Pune, 1999
August 2003

ACKNOWLEDGEMENTS

I take this opportunity to express my deepest gratitude to Dr. Eyassu Woldesenbet, my advisor, for all the support and guidance he has given me throughout my graduate study and thesis work. His suggestions and constant encouragement helped me a lot.

I am grateful to my committee members, Dr. Su-Seng Pang, Dr. Guoqiang Li and Dr. Linbing Wang who have been helpful and generous with their time and expertise to evaluate my thesis.

I am grateful to my parents and my sister, for the tremendous amount of inspiration and moral support they have given me since my childhood. My special thanks goes to Mr. William VanBeuningen and Mrs. Susan VanBeuningen for their support and encouragement in my work. I also thank to my friends Nikhil, Varshni, Sanjay and Shanti for their help in my work and all my other friends at Louisiana State University, Baton Rouge and Southern University and A & M College, Baton Rouge who helped me directly and indirectly in my thesis work.

TABLE OF CONTENTS

LIST OF TABLES

LIST OF FIGURES

ABSTRACT

The vast differences in strength, ultimate strain and modulus during high strain rate (HSR) deformation of materials have been a very long-standing subject of engineering interest. This thesis deals with characterization of mechanical properties of two composite materials, balanced angle-ply graphite epoxy laminates (fibrous composite) and syntactic foams (particulate composite). The focus of this study is to compare the mechanical properties of these composite materials at high strain rates and quasi-static conditions and to find out the effects of failure modes on HSR mechanical properties of these materials.

Split Hopkinson Pressure Bar (SHPB) apparatus is used for the HSR testing of balanced angle-ply IM7/8551-7 graphite/epoxy laminates and syntactic foams at varying strain rates, ranging from 500 s^{-1} to 1700 s^{-1}. Graphite/epoxy laminates with seven different fiber orientations including longitudinal and transverse are used in this study. Syntactic foams of four different densities are used in order to observe the density effect on the HSR properties. The aspect ratio (L/D) of all the specimens is kept equal to one. Failed specimens are consequently observed under optical and scanning electron microscope in order to understand the fracture modes of these materials.

The results of the tests on both materials demonstrate considerable increase in peak strength and the elastic modulus under HSR. It is also observed that the failure strain values vary considerably with increasing strain rate. Fiber orientation, in case of balanced angle-ply graphite epoxy laminates and density in case of syntactic foams are found to influence the HSR mechanical properties and strain rate sensitivity of peak stress. Delamination caused by edge effects is the prominent mechanism of failure for graphite/epoxy specimens whereas vertical cracking through cenospheres is recognized to be the dominant mode of failure for syntactic

foam specimens under HSR testing conditions. These results are essential for conducting realistic numerical simulations for safe design of structures.

1 INTRODUCTION

1.1 General Introduction

Polymers reinforced by second phase have a number of attractive material properties such as high specific stiffness and strength, fatigue behavior, tailorability, and corrosion resistance which make them suitable for use in structural applications. The second phase (reinforcement) in these kinds of composites can be of any form such as fibers, particles or flakes. A major concern in the use of these composite materials is their susceptibility to damage resulting from effects of rapidly applied loads occurring over a short period of time.

Graphite/epoxy is one of the most popular materials of this class. A large number of its applications such as armor, naval and aerospace structures using graphite/epoxy composites involve dynamic loading. The stress wave generated during an impact can travel at velocities considerably greater than the velocity of the projectile/ impactor and can cause damage to the body. Since the material deformation and failure processes are greatly influenced by these loading conditions, the inherent multiphase structure of composites result in complex failure/ fractures of constituent elements. The failure mechanisms are obviously more complex than those of monolithic materials. Composites material constructions involved in these applications almost always utilize the static properties in their material selection and design, because of unavailability of dynamic properties. The use of static properties in the study of structures that undergo dynamic loading can produce excessive design weight or cause unexplained and untimely failure.

Another example of these kinds of reinforced polymeric materials is syntactic foam, which is produced by the mechanical mixture of cenospheres (hollow particles) in polymeric resin matrix. These materials are classified as close pore foams, as the porosity in syntactic

foams exists in the form of hollow particles. Syntactic foams are commonly used as core materials for sandwich structured composites. High specific compressive strength, lower moisture absorption coefficient compared to the open cell structured foams, high tailorability of mechanical properties of these materials make them suitable for weight sensitive structural applications. Applications of these type of composites in aircraft and marine structure components and, shock absorbing packaging require strong understanding of the dynamic mechanical properties of syntactic foams. This is necessary because the impact loading conditions may significantly alter the mechanical response of the material. Hence, syntactic foams should also be characterized for high strain rate properties by carefully controlled experiments.

1.2 Previous Work

A variety of techniques have been tried till date to achieve medium and high strain rate response of composite materials. Barr and Bouamarata [1] have studied the flexural dynamic properties of fiber reinforced concrete materials using a drop weight apparatus. Here they found that as the fiber content was increased progressively from 0.25% to 1.0% fiber content, the number of impacts required to cause failure of the specimens increased. Dynamic three-point flexure tests have been performed by Boukhili [2] on glass fiber reinforced polyesters at strain rates of up to 80 s^{-1}. Results obtained from these tests include that shear strength and flexural strength increase with loading rate, with rate effects greater in glass-polyester than in glass-epoxy. Limited data on tensile behavior of fibrous composites at high strain rates have been obtained by Daniel [3] using the expanding ring technique. These tests carried on graphite-epoxy specimens at the strain rates of 500 s^{-1} showed that there is an increase in longitudinal, transverse in-plane shear moduli, as well as higher in-plane and transverse strengths. For a direct

determination of material properties at strain rates between 200 and $10^4 s^{-1}$, the most widely used technique used for testing metals is the Split Hopkinson Pressure Bar (SHPB), first introduced by Kolsky [4]. By using the SHPB technique, the effects of strain rate on tensile properties of glass-epoxy angle-ply laminates were investigated by Stabb and Gilat [5]. They showed that the tensile strength is higher in dynamic tests and more pronounced when specimen made of smaller angles are used. Gilat et al. [6] studied the strain rate sensitivity of IM7/977-2 carbon/epoxy composite under dynamic tensile loading and found the material to be highly strain rate sensitive. In particular, they have found that the composite is more strain rate sensitive at shallower angles. Lataillade [7] has investigated the tensile strain rate behavior of E-glass/epoxy ($\pm 45^o$) cross-ply laminates using a servo-hydraulic testing machine and a Hopkinson pressure bar. Results of this study show that the mechanical parameters related to interlaminar shear loading follow a logarithmic evolution law and damage initiation of composite materials under interlaminar shear loading increases at low and intermediate strain rates. Even though these studies mentioned here represent some aspects of dynamic properties investigations of angle-ply laminates, there are only limited data of dynamic compressive properties of balanced angle-ply laminates.

Detailed studies of quasi-static properties of syntactic foams can be found in the literature. Particularly, large number of studies on compressive [8-13] tests of these materials is available in the published literature. Dynamic tests are also conducted in industry to characterize the impact energy behavior of a variety of rigid polymers using drop weight tower [14] or simulated head impact using dynamic impact sled [15]. High strain rate mechanical properties of metallic foams have been studied by many researchers using the Split Hopkinson Pressure Bar (SHPB) technique [16-19]. These studies suggest that compressive flow stress of the Al-foam is a function of the relative density but does not exhibit strain rate sensitivity. High strain rate

compressive behavior of a rigid polyurethane foam with various densities is determined by Chen et. al. [20]. They found the peak stress to be strain rate sensitive and expressed it in terms of the square of the foam density. Tensile and compressive properties of polystyrene bead (PSB) foams at various temperatures and strain rates are studied extensively by Rinde et. al. [21]. Some of the previous studies on the dynamic properties of cellular materials such as honeycombs can also be found in the published literature [22 & 23]. These studies found an increase of 20 to 70% in the dynamic crush strength at impact velocities of 30 m/s. Energy absorption characteristic of variety of composite materials, sandwich structures, polymeric foams and metallic foams with different densities have been evaluated under high strain rates by various other researchers as well [24-27].

1.3 Present Work

The intent of this thesis is to determine material properties of practically useful materials for better design of composite material structures in high strain rate applications. Such data are essential for conducting realistic numerical simulations for safe design of structures. Two composite materials, balanced angle-ply graphite epoxy laminates (fibrous composite) and syntactic foams (particulate composite) were chosen for study. The need for testing balanced angle-ply laminates has been explained in the following paragraph whereas almost lack of data for high strain rate mechanical properties of syntactic foams is the driving force behind the study of these novel sandwich core materials.

Vinson and Woldesenbet [28] have conducted a series of tests for the compressive mechanical properties of unidirectional graphite/epoxy laminate composites at various off-axis angles. Their study showed that specimens having 60^{o} off-axis fiber orientation failed in shear mode giving lower amount of stress and strain values than expected. This was attributed to the

in-plane shear stress coupling. It is very important to study the high strain rate effects on balanced angle-ply laminates because they behave as orthotropic layers with respect to in-plane forces and strains, that is, there would be no coupling between the normal stress (or forces) and shear strain. This is possible when the terms A_{16} and A_{26} in an extensional stiffness matrix, [A], are zero, as shown in Equation (1).

$$\begin{Bmatrix} N_x \\ 0 \\ 0 \end{Bmatrix} = \begin{bmatrix} A_{11} & A_{12} & 0 \\ A_{21} & A_{22} & 0 \\ 0 & 0 & A_{66} \end{bmatrix} \begin{Bmatrix} e_x^0 \\ e_y^0 \\ g_{xy}^0 \end{Bmatrix} \qquad (1)$$

where N_x represents force per unit width applied in the x direction and e_x^0, e_y^0 and g_{xy}^0 represent mid-plane strains in the respective directions.

In this thesis, a systematic study of strain rate effects on the response of symmetric balanced angle-ply graphite/epoxy laminates is presented. The compressive SHPB technique is used to develop strain rates of 500 s^{-1} to 1500 s^{-1}. Solid cylindrical specimens with an aspect ratio (L/D) of 1, and fiber orientations of 0^o (longitudinal direction), $\pm 15^o$, $\pm 30^o$, $\pm 45^o$, $\pm 60^o$, $\pm 75^o$ and 90^o (transverse direction) are used for the tests.

In addition to the above, schematic study of high strain rate properties of syntactic foams with four different densities is conducted at the strain rates up to 1800 s^{-1} with the aid of SHPB. Solid cylindrical specimens of aspect ratio of 1 are used for the tests.

In both cases, the results of the high strain rate tests are subsequently compared to quasi-static tests. Significance of strain rate effects on the values of compressive strength, failure strain and compressive modulus has been observed. Another objective of the present study is to provide insight into energy absorption features of the syntactic foam under high strain rate conditions for various densities of the foam. Also microscopic observations regarding the failure

mechanisms for both types of composite materials are presented. Various conclusions regarding the relationships between damage mechanisms and high strain rate mechanical properties of tested materials are drawn.

2 SPLIT HOPKINSON PRESSURE BAR APPRATUS AND PROCEDURE

This chapter introduces and fully develops the theory behind compressive Split Hopkinson Pressure Bar (SHPB) testing. It begins by developing the equations for calculating the specimen stress, strain, and strain rate. This chapter then presents a typical SHPB setup for the compressive high strain rate test at the Composite Materials Laboratory at Louisiana State University. The basis for various testing precautions and data acquisition are described in brief. The basic procedure of performing the test is described at the end of the chapter.

The SHPB is the most commonly used apparatus for determining material properties at high strain rates. The principal application of the SHPB has been in the study of the transient response of materials to dynamic loading. The theory governing the specifics of SHPB testing method has been around for decades.

The SHPB apparatus consists of two pressure bars of constant cross section A_o, elastic modulus E, and density ρ as shown in Figure 1. Here a test specimen can be seen as a sandwich between two bars. The term 'c' in Figure 1 is formulated as 'C_o' in the following paragraph and is the wave velocity in any particular material. Since the two bars are identical, it is only necessary to consider one of them in developing the equation of motion governing axial vibration. Typically the length-to-diameter ratio of the pressure bar used in SHPB is ten or greater [29].

It can be shown that C_o is the wave velocity and can be calculated from Equation 2,

$$C_o = \sqrt{E/r} \qquad (2)$$

where E and ρ are the bars elastic modulus and mass density, respectively.

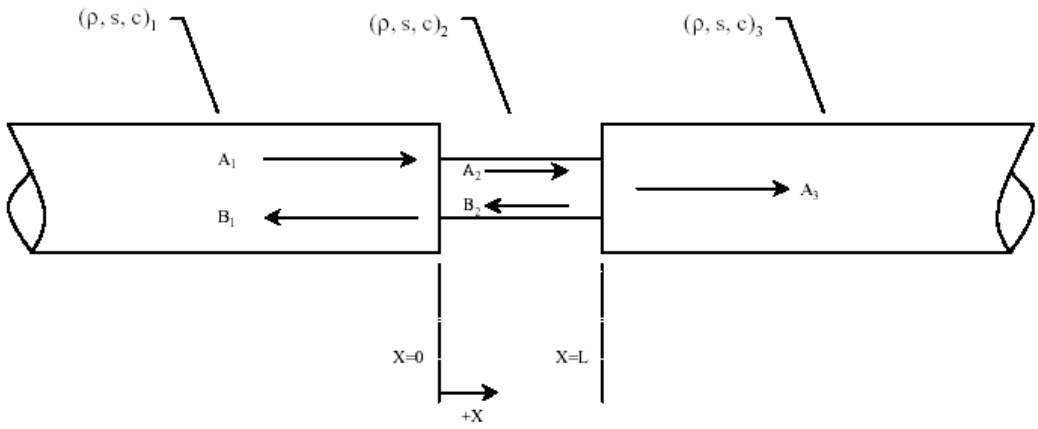

Figure 1 Schematic of materials properties in SHPB

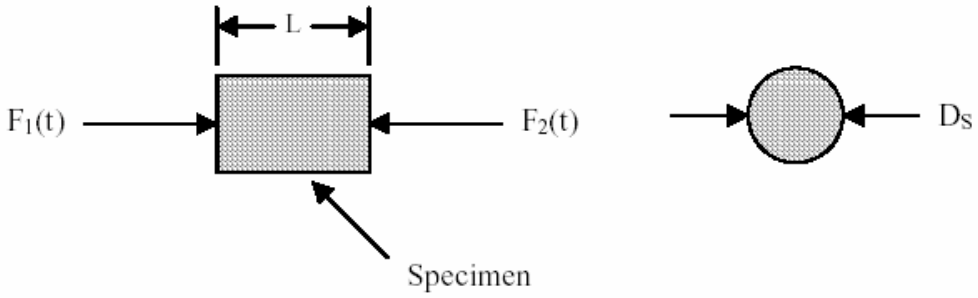

.

Figure 2 Schematic of cylindrical specimen

2.1 Calculation of The Specimen Stress, Strain-Rate and Strain

The following section derives the expressions for calculating specimen stress, strain rate, and strain.

2.1.1 Specimen Stress

The average stress in the specimen can be expressed in terms of the forces exerted on each surface of the specimen. A schematic representation of any specimen is shown in Figure 2. When the specimen is sandwiched between the pressure bars forces $F_1(t)$ and $F_2(t)$ exist on the

specimen of instantaneous diameter D_s. The average force on the specimen is given by Equation 3.

$$F_{AVG}(t) = \frac{F_1(t) + F_2(t)}{2} \tag{3}$$

and hence the average stress on the cylindrical specimen is given by Equation 4.

$$\sigma_{AVG} = 4F_{AVG}(t) \Big/ pD_s^2 \tag{4}$$

The forces $F_1(t)$ and $F_2(t)$ acting at the specimen surfaces are due to the pressure bars. For a specimen in dynamic equilibrium, the forces at the ends of the pressure bars may be expressed in terms of the incident and reflected pressure bar strains as given in Equation 5.

$$F_1(t) = \frac{E}{4}[\varepsilon_I(t) + \varepsilon_R(t)]\ p\ D_{Bar}^2 \tag{5}$$

$$F_2(t) = \frac{E}{4}\varepsilon_T(t)\ D_{Bar}^2 \tag{6}$$

where D_{BAR} is the diameter of the pressure bars. Substituting Equations 3-6 into Equation 4 results in an expression for the average stress on the specimen in terms of the pressure bar strains

$$\sigma_{AVG}(t) = ED_{Bar}^2\ [\varepsilon_I(t) + \varepsilon_R(t) + \varepsilon_T(t)] \Big/ 2D_s^2 \tag{7}$$

If the specimen deforms uniformly, the strains in the incident bar are equal to the strain in the transmitter bar as depicted in Equation 8.

$$\varepsilon_I(t) + \varepsilon_R(t) = \varepsilon_T(t) \tag{8}$$

And the expression for the average specimen stress can be reduced to Equation 9.

$$\sigma_{AVG}(t) = \varepsilon_T(t)\ ED_{Bar}^2 \Big/ D_s^2 \tag{9}$$

This equation shows that the specimen stress is proportional to the amplitude of the strain transmitted through the specimen into the transmitter bar.

2.1.2 Specimen Strain-Rate and Strain

The average strain rate is defined as the average strain divided by the time over which the straining occurs. Strain indicates displacement, which divided by time indicates velocity. The specimen strain rate may be calculated from the pressure bar-specimen interface velocities. These interface velocities can be calculated from the strains in the pressure bars. To derive the expressions for the specimen strain rate and strain in terms of the pressure bar strains, the equation of motion for the pressure bar can be given by Equation 10,

$$\frac{C_0^2 \partial^2 u_1}{\partial y^2} = \frac{\partial^2 u_1}{\partial t^2} \tag{10}$$

Recognizing that for harmonic waves $\partial^2 u_1 / \partial t^2$ is equal to $\partial v / \partial t$ where v is the particle velocity, and that

$$E \frac{\partial}{\partial y} [\partial u_1 \Big/ \partial y] = \partial p \Big/ \partial y \tag{11}$$

where p is the stress across the cross section, the equation of motion can be rewritten in terms of the pressure and velocity across the bar cross section as

$$- \frac{\partial p(y,t)}{\partial y} = \rho \frac{\partial v}{\partial t} \tag{12}$$

Notice from equation 12 that to solve for the particle velocity in a bar requires knowledge of the pressure in the bar. If we assume a positive traveling harmonic wave of the form

$$P(y, t) = Pe^{i(\omega t - ky)} \tag{13}$$

where P is the amplitude of the pressure, ω is the frequency, t is the time, k is the wave number and is defined as $k = \omega / C_0$, and y is the spatial location of the wave an expression for the instantaneous particle velocity can be derived. Taking the first derivative of Equation 13 with respect to y, one arrives at

$$\frac{\partial p(y,t)}{\partial y} = - ikPe^{i(\omega t - ky)} \tag{14}$$

Substituting this derivative into Equation 12 and pre-multiplying the RHS of Equation 10 by the heavyside operator, one attains

$$ikPe^{i(\omega t - ky)} = \rho\, iw\, v(y,t) \tag{15}$$

which can be solved for the particle velocity, given by Equation 16.

$$v(y,t) = \frac{k}{rw} Pe^{i(\omega t - ky)} \tag{16}$$

Substituting the expression for k and $p(y,t)$ back into the expression for the particle velocity yields as in Equation 17.

$$v(y,t) = \frac{1}{rC_0} P(y,t) \tag{17}$$

where P is the pressure across the cross section. For a uniaxial state of stress, the pressure is equal to the stress over the pressure bar cross section. Therefore, $p(y,t)$ can be written in terms of the bar strain by Equation 18.

$$P(y,t) = \varepsilon(y,t)E \tag{18}$$

By substituting Equation 17 into Equation 16 yields an expression for the particle velocity in terms of the bar strain as given in Equation 19.

$$v(y,t) = C_0\, \varepsilon(y,t) \tag{19}$$

For a negative traveling wave the particle velocity is expression given by Equation 20.

$$(y,t) = -C_0\, \varepsilon(y,t) \tag{20}$$

With expressions for the particle velocity in terms of the pressure bar strains, specimen strain rate can be calculated rather simply. The average strain rate at any given time is given by Equation 21.

$$\frac{de}{dt} = (v_{interface2} - v_{interface1}) \,/\, L \tag{21}$$

The velocity at interface 1 is comprised of the incident (+ traveling wave) and the reflected (- traveling wave) given as in Equation 22.

$$v_{interface1} = C_0\, e_I - C_0\, e_R = C_0\,(e_I - e_R) \tag{22}$$

To calculate the velocity of the second interface only requires knowledge of the strain transmitted into the pressure bar. Since the transmitted wave propagates in the positive direction, the velocity of interface two appears as a positive quantity in Equation 23.

$$v_{interface2} = C_0\, e_T \tag{23}$$

By substituting these interface velocities into the expression for the specimen strain rate yields an expression for the specimen strain rate in terms of the pressure bar strains expressed by Equation 24.

$$\frac{de_s}{dt} = \frac{-C_0(e_T - e_I + e_R)}{L} \tag{24}$$

where the negative sign represents compression. If the specimen deforms uniformly such that

$$e_I(t) + e_R(t) = e_T(t) \tag{25}$$

The expression for the specimen strain rate can be reduced to Equation 26.

$$\frac{de_s}{dt} = -\frac{2C_0}{L}\int e_R \tag{26}$$

which can be simply integrated to yield the specimen strain as given in Equation 27.

$$e_s(t) = \frac{2C_0}{L}\int e_R(t)dt \tag{27}$$

Though a bit lengthy to arrive at, the equations for calculating specimen properties are rather simple to use.

2.2 SHPB Setup at Louisiana State University

A SHPB test setup was designed and built for dynamic type compression testing of various materials for strain rates exceeding several hundreds per second. It basically consists of a pneumatic loading device, which includes a pressure chamber, gun barrel and release valve. It also consists of incident and transmitted pressure bars and a striker bar supported by Teflon bearings. It is the yield strength of the incident pressure bar that limits the maximum attainable specimen stress, since the equations developed in previous section are valid only for an elastic bar. Before choosing a pressure bar material, careful consideration must be given to the desired sample stress levels. To achieve very high strain rates requires reducing the bars' cross sectional area, and consequentially diameter. It is often desirable to have several different pressure bars; each suited for testing materials in a certain range of strain rate and strain. Choosing an appropriate length for the bars requires that two conditions be met:

- Length-to-diameter ratio meets requirements for one-dimensional propagation theory
- Length of bar is at least twice that of the compressive pulse generated during impact

Most texts suggest that the bar have a length-to-diameter ratio of at least ten [29]. The length of the pressure bar affects how much strain a specimen may see, since strain is related to the total pulse duration, which is directly related to the length of the pressure bar. To measure the incident and reflected pulses independently requires that the bar length exceed twice the length of the impact pulse. The pressure bars available at Composites Laboratory at Louisiana State University, have properties shown in Table 1.

The present study is carried out by using a striker bar and pressure bars made from maraging steel having very high values of yield strength in order to withstand a very high impact velocity. These pressure bars are mounted on a rigid beam. Solid cylindrical composite

specimens with intended dimensions are sandwiched between the two pressure bars. The overall specimen dimensions are required to be small to minimize the effects of longitudinal and lateral inertia and wave dispersion within the specimen. Strain gauges (with resistance of 350 Ohms and Gauge Factor of 2.10 at room temperature) are mounted on incident and transmitter pressure bars at the distance of 18.5 cm from the junction ends of both pressure bars.

The schematic diagram of the SHPB apparatus is shown in Figure 3. The loading pulse in these experiments is initiated by an axial impact on the free end of the input bar by striker bar, which is accelerated through a gun barrel. To control the velocity of the striker bar to a desired velocity, the air pressure is controlled by regulators.

After an impact caused by the striker bar, an elastic compressive wave of constant amplitude and a finite duration is generated in the input pressure bar. The incident pulse wavelength can be adjusted by using striker bars of different lengths, as the pulse in the incident bar is twice the length of the striker bar. The amplitude of the pulse is also directly proportional to the impact velocity of the striker bar [30]. When the compressive loading pulse in the incident pressure bar reaches the specimen, some part of the pulse gets reflected from the specimen-input bar interface, while some part is transmitted to the transmitted bar. The magnitudes of these

Table 1 Properties of Pressure Bars

Material	Yield Strength (MPa)	Wave Speed (m/s)	Length of Striker Bar (m)	Length of Incident Bar (m)	Length of Transmitter Bar (m)
Maraging AISI Grade 18Ni (350)	2363	4980	0.152	1.22	0.61
Al 6061-T913	455	5060	0.152	1.22	0.61
Inconel 718	1100	4940	0.152	1.22	0.61

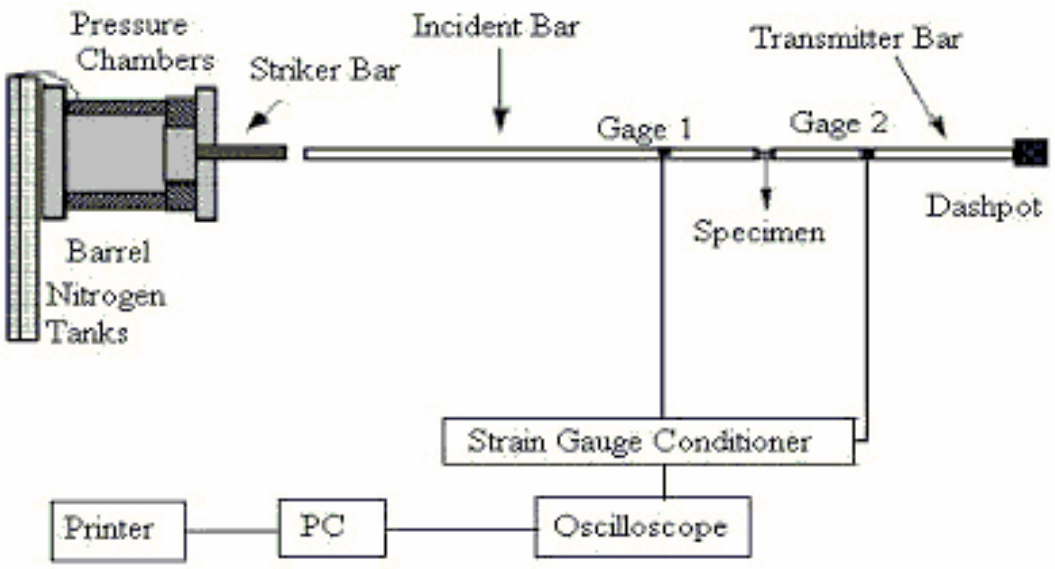

Figure 3 Schematic of Split Hopkinson Pressure Bar

reflected and transmitted pulses will decide the physical properties of the specimen. High numbers of internal reflections are experienced in the short specimen during the duration of the loading pulse since the loading pulse time is long compared to the wave transit time in the specimen. The reflections cause the stress distribution in the specimen to be uniform [31]. The proof is provided in next chapter of this thesis. The strain gauges located on the pressure bars are connected to a signal bridge conditioner. The strain gauge signal is amplified and recorded by digital processing oscilloscope. This data from the oscilloscope is transferred to a personal computer for further data reduction.

The strain rate ($\dot{e}$), strain (ε) and stress (σ) of the specimen are given by Equations 26, 27 and 9 respectively. From these equations, it is clear that the strain is obtained by integrating the reflected pulse and the stress in the specimen from the transmitted pulse.

2.3 Testing Precautions

It is assumed that one-dimensional theory applies for all calculations in this thesis. Geometry plays a major role in determining whether a wavefront can be described by one variable or not. As was presented in the previous section, the bar length-to-diameter ratio needs to be greater than ten. The most important experimental factor influencing the nature of wave propagation is bar alignment. If the striker bar impacts the incident bar at an angle, a non-uniform wave distribution will exist across the bar cross-section, and hence a multi-dimensional strain field will result. This also holds true for the alignment of the incident bar with the transmitter bar. By carefully aligning the striker bar with the incident bar such that the two remain in the same plane, a one-dimensional wavefront can be attained experimentally.

The equations leading to specimen stress, strain rate and strain were greatly reduced by assuming that the specimen deforms uniformly over its length. Many investigators have been concerned with this assumption and have dedicated lengthy studies to it. This paragraph describes problems with assuming that the specimen deforms uniformly, and how most investigators circumvent these problems. During the compression test the specimen shortens and expands. At the pressure bar-specimen interface a frictional constraint exists due to this radial expansion. The frictional effects are highest when the specimen is at rest, and then reduce once the static friction is broken and the specimen starts sliding. If the ends are restrained in the beginning of the test, the middle section of the specimen must deform. This results in a barrel shaped specimen, clearly not uniform. By applying thin films of lubricant at the interfaces, this frictional constrain can be greatly reduced. Hence, in the present study molybdenum disulphide lubricant is applied.

Specimen diameters are usually smaller than the pressure bar diameters, since the sample expands during the test. It is important to align the centerlines of the sample and pressure bars to load the transmitter bar uniformly. Simpson designed and built a clever device for centering the sample on the pressure bar [29]. The user simply slides the alignment tool over the end of the pressure bar, followed by placing the sample into the alignment tool as shown in Figure 4.

In the present work, we have used the specimens of sizes slightly smaller than bar diameters due to the low Poisson's ratio of the specimen being tested. A thick flexible polymeric pipe was used to keep the specimen in place while being tested. It is similar to above technique. The thin layer of lubricant on the end of the sample is enough to hold the sample in place, while the user removes the alignment tool and slides the other pressure bar against the opposite sample end.

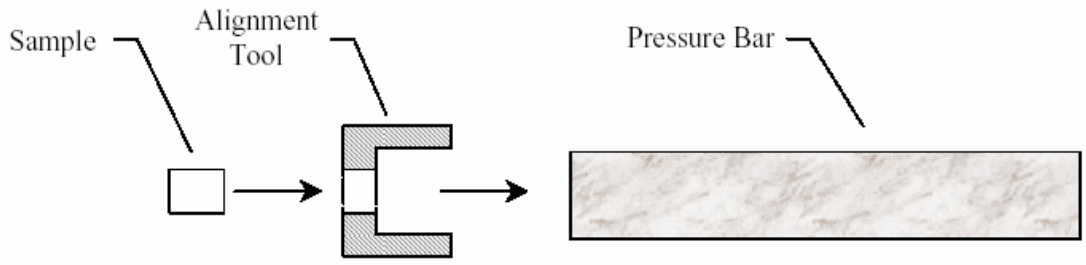

Figure 4 Technique for aligning sample with pressure bars

2.4 Testing Procedure

To perform a SHPB test, certain decisions and preparations need to be made. Firstly, the investigator needs to decide which specimen properties are of interest. Specifically, the expected strain rate and total strain must be determined prior to any testing. After deciding on the desired specimen properties, specific steps are taken to ensure that those properties are attained in the test. A typical procedure to be followed for performing every test is given as follows:

1. Ensure alignment of Bars
2. Check specimen dimensions carefully and apply lubricant on it’s ends
3. Sample and timer positioning
4. Pressure valves in appropriate position
5. Adjust oscilloscope and strain gauge conditioner parameters
6. Set pressure parameters
7. Fire projectile
8. Transfer data from oscilloscope to PC
9. Reduction of data in Microsoft Excel
10. Plotting stress-strain curve to check validity of the test.

3 EXPERIMENTAL INVESTIGATION

3.1 Materials and Sample Preparation

3.1.1 Fabrication of Balanced Angle-Ply Graphite/Epoxy Laminates

The material used is an IM7/8551-7 graphite/epoxy composite. The laminate included 76-layers of symmetric balanced angle-ply lay-up. The prepreg lay-up is cured in a compression molding press by a two-step curing process under vacuum as per manufacturer's suggested curing process as described below. Laminated sheets with the fiber orientation of 0^o, $[\pm 15^o]_s$, $[\pm 30^o]_s$, and $[\pm 45^o]_s$ and with dimensions of 25 cm x 25 cm are produced.

The compression molding is used for the fabrication and is carried out in the following sequence:

1. The IM7/8551-7 graphite/epoxy laminae are stacked in proper sequence (as shown in Figure 5) and rolled simultaneously to remove entrapped air between them.
2. This laminate is held at a full vacuum for 30 minutes.
3. A load of 1150 kg. is rapidly applied and the compression molding plates heated to temperature of $115^oC \pm 5^o$; the pressure maintained constant by using compression moldings machine.
4. The laminate is held at 115^oC for 1 hour with the 1150 kg load applied.
5. The load is increased to 1600 kg., with increase in the temperature to $180^oC \pm 5^o$. At this stage the vacuum is vented.
6. The laminate is held at 180^oC for 1.5 hours.
7. A full vacuum is applied turning off the heated platens. This allows the laminate to cool to 95^oC and get consolidated.

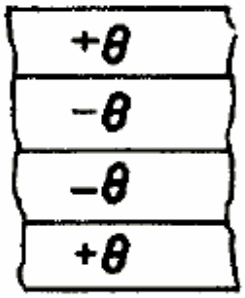

Figure 5 Laminate lay-up

8. The plate is cooled to room temperature on a flat surface and then removed from the vacuum bagging.

The individual specimens are then prepared from the finished laminate. The laminate is sectioned by using water-cooled masonry saw equipped with diamond grit blade, which usually produces no delamination or rough surfaces. For static and dynamic testing of $[\pm 30^o]_s$, $[\pm 45^o]_s$, $[\pm 60^o]_s$, $[\pm 75^o]_s$, and $[90^o]_s$, solid cylinders with 0.952 cm diameter and of the same length are core drilled. In order to assure specimen failure, a diameter of 0.673 cm is selected for the dynamic testing of $[0^o]_s$ and $[\pm 15^o]_s$ samples. The average fiber volume fraction is found to be approximately 52% in burn-off tests. The faces of the specimens are polished with 400- grit polish paper. Figure 6 shows a typical micrograph of a manufactured graphite epoxy specimen. It is evident from this figure that fibers are totally wetted by the matrix with no visible porosity.

3.1.2 Fabrication of Syntactic Foam

Syntactic foams are two-phase materials having cenospheres dispersed in a matrix material. Structure of syntactic foam is shown in Figure 7. It is possible to manufacture syntactic foams of different densities by keeping the volume fractions of cenospheres and the matrix resin constant. Cenospheres of different wall thickness but same outer radius can be selected for this

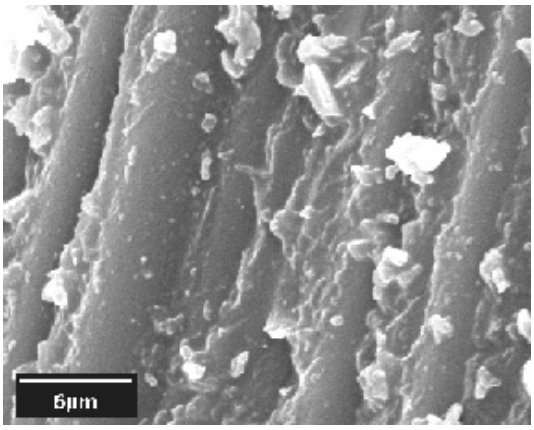

Figure 6 Scanning Electron Microscope (SEM) Image of a manufactured graphite/epoxy specimen.

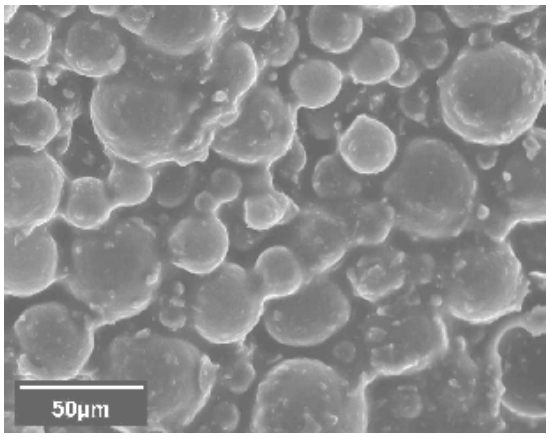

Figure 7 Structure of syntactic foam.

purpose. As the first option, matrix-cenosphere volume fractions can be changed to achieve a specific foam density. However, the same density can also be achieved at a different matrix-cenosphere volume fraction ratio by selecting cenospheres of different wall thickness. Syntactic foams obtained from both routes would have the same density but different mechanical properties. In the present study cenospheres of four different wall thicknesses have been used to fabricate syntactic foams. All types of cenospheres have nearly the same particle size distribution. However, there is considerable difference in their density, due to the difference in the wall thickness. Matrix resin composition, matrix-cenospheres volume fractions and processing parameters for all types of syntactic foams have been kept the same. This would allow the observed difference in the mechanical properties of the syntactic foams be directly related to the variation in the wall thickness of cenospheres. Details of raw materials used for the fabrication of syntactic foam are given below.

3.1.2.1 Matrix Resin

Based on a comparative study of various commercially available epoxy resins, D.E.R. 332, a di-epoxy resin, manufactured by DOW Chemical Company is selected for the study. This

resin is called diglycidyl ether of bisphenol A (DGEBA). Chemical name of this resin is 2,2-bis[4-(2'3' epoxy propoxy) phenyl] propane.

3.1.2.2 Diluent

A diluent is added to lower the viscosity of the resin mix. It is difficult to mix large volume of cenospheres in the resin if the resin viscosity is very high. Adding 5% by weight diluent C_{12}-C_{14} aliphatic glycidyl ether, commercially known as ERISYS-8, brings down the viscosity of the resin from about 4000 cps at 20°C to about 2000 cps at the same temperature. The diluent was supplied by CVC Specialty Chemicals. Additional effects of diluent addition are lowering the modulus of the epoxy with a corresponding increase in ductility. Average equivalent epoxide weight (EEW) of the diluent is 285. For a 95 wt% resin and 5 wt% diluent mixture the EEW is calculated to be 17.75.

3.1.2.3 Hardener

A polyfunctional aliphatic amine triethylene tetramine (TETA), $C_6H_{18}N_4$, is used as a curing agent. This chemical is commercially known as D.E.H. 24 and manufactured by DOW Chemical Company. Molecular weight of this hardener is 146.4 and weight per active hydrogen is 24.4. Phr (parts per hundred parts of resin) of amine for 95:5% by weight resin-diluent mix is calculated to be 13.74. For the selected combination of epoxy resin and hardener the curing schedule is to gel at room temp and then post cure at 100°C for 1-2 hrs.

3.1.2.4 Cenospheres

Five different types of borosilicate glass cenospheres are used for the fabrication of syntactic foam specimens. These cenospheres were manufactured and supplied by 3M under the trade name "Scotchlite". Distribution of outer diameter of all types of cenospheres is nearly the

Table 2 Properties of cenospheres used to fabricate syntactic foam slabs.

Cenosphere Type	Cenosphere Density (kg/m^3)	Mean Cenosphere Diameter (μm)	Calculated Radius Ratio η
S22	205	35	0.922
S32	320	40	0.907
S38	380	40	0.888
K46	460	40	0.863

same, but the internal diameter is different. Cenosphere wall thickness can be related to a parameter named Radius Ratio, η, which is given by Equation 28.

$$\eta = \frac{r_1}{r_0} \tag{28}$$

Where r_1 is the internal radius and r_0 is the outer radius of the cenosphere. Increase in η corresponds to a decrease in wall thickness, which leads to a decrease in true particle density of cenosphere. Therefore, cenospheres having higher η value give rise to lower density syntactic foams and vice versa. Mean particle size, true particle density and radius ratio values of selected cenospheres supplied by the manufacturer are given in Table 2.

3.1.2.5 Mold

Stainless steel molds having inner dimensions of $228 \times 228 \times 13$ mm^3 are used for casting the syntactic foams. No vacuum or pressure is applied during the casting or curing of syntactic foam slabs.

3.1.2.6 Mold Release Agent

Dow Corning 111 Sealant and Lubricant is used as a release agent in the molds. This lubricant is silicone based white translucent gel. Selection of this release agent is based on its

service temperature range of –40 to 204°C and bleed characteristics, 0.5% in 24 hrs at 200°C. Specific gravity of this release agent is 1.0.

3.1.2.7 Syntactic Foam

Volume fraction of cenospheres is maintained at 0.65 in all types of syntactic foams. Fabrication of syntactic foams is carried out in a two-step process, mixing and casting. First the resin and diluent are mixed and heated to 50°C to further reduce the viscosity of the mix. Hardener is then added and stirred thoroughly, followed by cenospheres addition. The mixed is stirred gently using wooden stirrers to minimize the damage to cenospheres during the mixing process. The slurry like mixture is then cast in stainless steel molds and cured for at least 36 hrs at room temperature. Cast foam slabs are removed from the molds and post cured at 100±3°C for 3 hrs. Fabricated syntactic foams have some entrapped air due to mechanical mixing being the fabrication route. This entrapped air is termed as voids. Density and void volume fraction values of fabricated syntactic foams are presented in Table 3.

The cylindrical foam specimens of 0.952 cm in diameter and of the same length are core drilled. The specimen ends were then carefully polished with 400-grit polish paper. The diameter of the samples was slightly less than that of the bars (0.965 cm) and due to small Poisson's ratio of foam, the specimen diameter during deformation never exceeds the bar diameter within the

Table 3 Density and void volume fractions in the fabricated syntactic foams.

Cenosphere Type	Corresponding Foam Nomenclature	Syntactic Foam Density (kg/m^3)	Void Volume Fraction
S22	SF 22	493	6
S32	SF 32	545	9
S38	SF 38	575	10
K46	SF 46	650	6

strain levels carried out. Higher diameter of foams is selected in order to compress larger volume of syntactic foam and to reduce statistical scatter.

3.2 Experimental Details

3.2.1 Static Testing

3.2.1.1 Static Testing of Balanced Angle-Ply Graphite/Epoxy Specimens

This is performed in order to compare the high strain rate responses to quasi-static responses. The strain rates of about $0.001s^{-1}$ are obtained using MTS servo-hydraulic machine. The tests are conducted by compressing the cylindrical specimen between two hardened steel parallel plates. Typical setup for the static testing is shown in Figure 8. Three specimens of each type of laminate are tested to obtain consistent results. The sample size and geometry are the same as the test pieces used in the dynamic tests in the SHPB for graphite/epoxy laminate testing. These make samples and the testing equipment different from what the American Society for Testing Materials (ASTM) suggests for static tests. Therefore, the static properties of the materials tested on the MTS machine could be different from the published data, depending on the type of the material. In light of the fact that quasi-static compression testing is still a subject of investigation with several researchers using different geometries and testing equipments, the use of the MTS machine with the same sample geometry as that used in SHPB test is felt to be the best way to proceed in obtaining the quasi-static properties of the materials studied.

3.2.1.2 Static Testing of syntactic foam specimens

ASTM standards have been followed wherever applicable in this work and have been given preference over any other standards that may exist on similar topics. ASTM D 695-96 is selected for the compression testing of syntactic foams. This standard is for unreinforced and reinforced rigid plastic type of materials. Some other researchers had also followed the same

Figure 8 Setup for quasi-static testing at Southern University, Baton Rouge.

standard according to earlier published experimental work [32]. Specimen and compression test details are given next.

Specimen dimensions recommended in ASTM D 695-96 for continuous cores are selected for syntactic foam specimens. The specimen cross section was 12.7×12.7 mm^2 and height is 25.4 mm. For compression testing MTS 810 Material Test System with microprocessor controlled data acquisition system is used. The rate of the crosshead movement is maintained at 1.3 mm/min. This makes the strain rate to be 0.0008 s^{-1}.

3.2.2 High Strain Rate Tests

These tests are conducted on a SHPB by varying the air pressure in the chamber from 100 psi to 400 psi. The velocity of the striker bar is shown to vary between 7 m/s and 20 m/s as a consequence of varying the pressure. The pressure bars mounted on a rigid beam and supported by Teflon rings are used to sandwich solid cylindrical test specimens between them. Similar

procedure was followed for tests on both kinds of material. Detailed description of the equipment and testing procedure for high strain rate testing has already been discussed in the previous chapter. The following section will discuss the Instrumental characterization and validity of these tests for the given materials under the testing conditions. Figure 9 shows a typical SHPB test set-up at LSU Composite Laboratory. Also a photograph of typical oscilloscopic record obtained during a test is shown in Figure 10.

A typical oscilloscope record for a syntactic foam specimen under testing obtained from SHPB experiments is shown in Figure 11. Waves for the incident and the transmitter bar can be observed in this figure. The transmitted wave records the stress history in the specimen. The first pulse, denoted by A, in the incident bar is the incident pulse; whereas the second pulse (B) is the reflected pulse. If the mechanical impendence of the specimen is less than that of the bar, the two pulses are opposite in sign, as shown in this figure. The transmitted pulse (C) through the syntactic foam specimen is lower than the incident pulse A. In the last part of the transmitted pulse, the stress decreases gradually compared to the incident pulse in a way similar to metallic specimens [33]. It can be noted that the magnitude of the reflected pulse is very high when compared to the transmitted pulse. Figure 12 shows similar kind of waves generated in bars during an experiment using a longitudinal graphite/epoxy specimen. It shows relatively lower magnitude of reflected pulse (which gives instantaneous specimen strain rate and strain) at much higher value of transmitted pulse (which gives specimen stress) in comparison with syntactic foam specimen, which fails at relatively much higher strain.

The plateau in the reflected pulse observed in Figure 11 indicates that the syntactic foam specimen deformed at a nearly constant strain rate for most part of the time during specimen deformation. For both kinds of materials, the strain rate for a given test varies as a function of

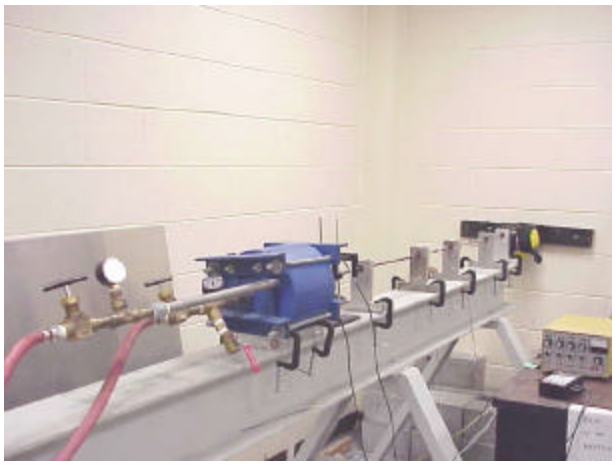

Figure 9 Split Hopkinson Pressure Bar Setup at LSU.

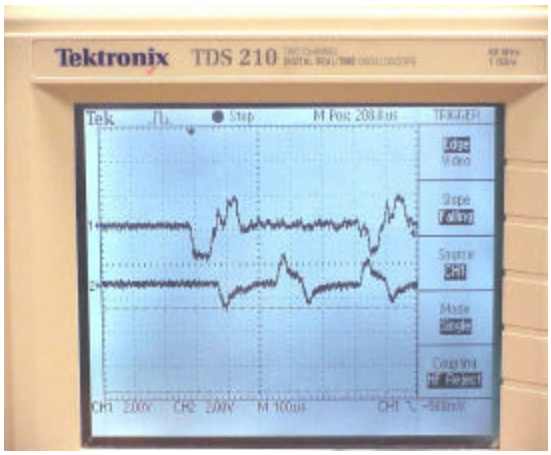

Figure 10 An oscilloscopic record obtained during a high strain rate test.

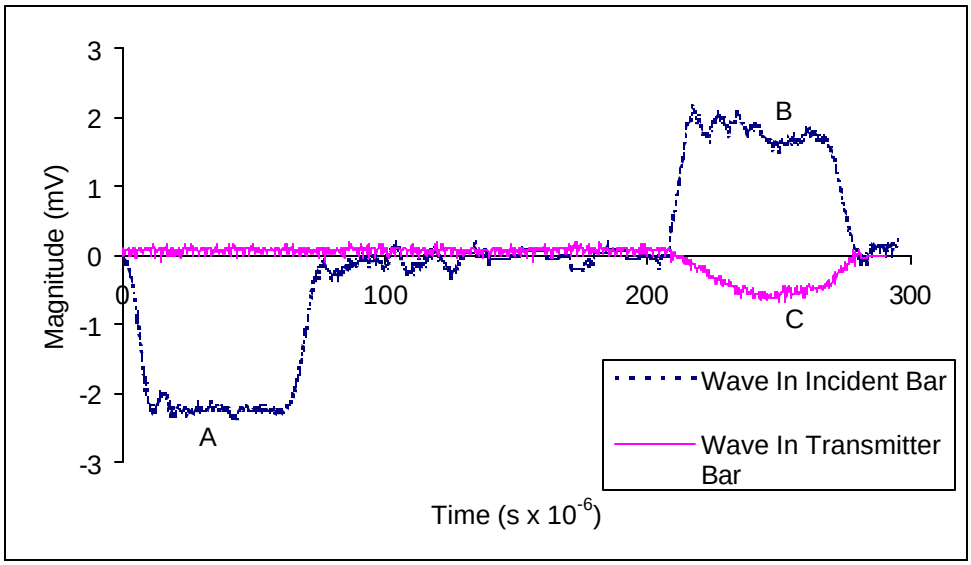

Figure 11 A typical oscilloscopic record for syntactic foam specimens.

time. Initially it increases from zero and remains relatively steady at a certain value as mentioned earlier. The average strain rate value is obtained and used to characterize the specific experiment.

3.3 Experimental Optimization and Validity of Testing

The stress wave produced initially because of impact from striker bar on one end of incident bar undergoes distorting wave phenomenon contrary to the basic assumption of uniaxial wave propagation. It is seen that the pressure wave dispersion is due to the wave velocities

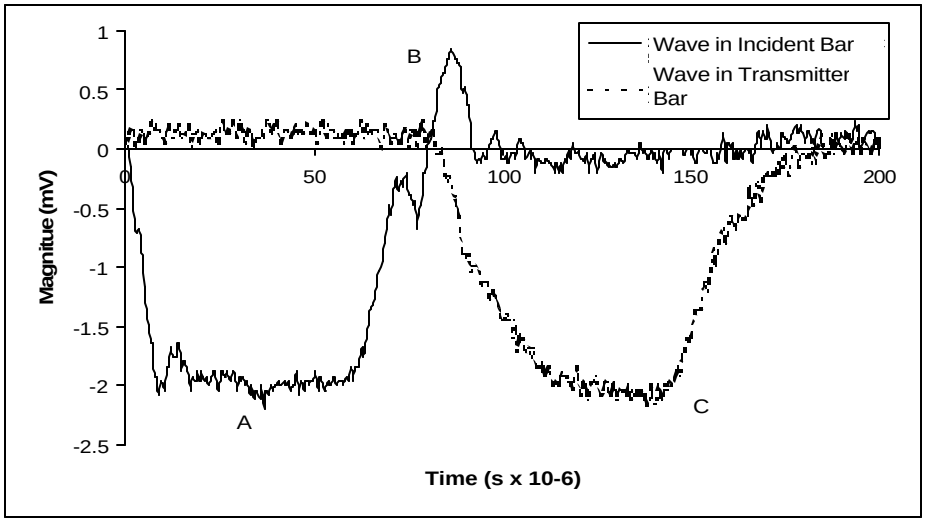

Figure 12 Typical oscilloscopic record for balanced angle-ply graphite/epoxy specimens.

dependence on frequency. It is recommended that the waves with narrower frequency bandwidth suffer less from distorting effects of dispersion and this can be obtained by increasing the rise time of the wave [29]. This shaping of impact pulse can be obtained by placing a yielding material (impact plenum) between the striker bar and the input bar. For our experimental work, two different mild steel plenums of 0.381 cm thickness are tested. It can be observed from the results in Figure 13 that tests conducted without plenum cause large oscillations in the bar. This effect is minimized with a 0.953 cm diameter plenum and can be further reduced with 0.673cm diameter plenum. The smaller diameter plenum is used for this study as it reduces the undesirable oscillations.

Based on the assumption that the dynamic force in both the incident and the transmitter bars are equal, the following equation can be written,

$$\varepsilon_T - \varepsilon_I = \varepsilon_R \tag{29}$$

where, ε_T, ε_I, and ε_R are pressure bar strains due to transmitted, incident and reflected pulse, respectively. This verification of dynamic equilibrium ensures that proper and valid tests are

conducted, Figure 14. The two curves match with each other to a large extent.

It is well known that the strain measurements by SHPB may not be completely reliable. In order to check the validity of this technique to measure the strain accurately, the strain measured directly from the specimen is compared to the strain calculated from the stress waves obtained from the strain gauges on the bars. A strain gauge is placed on a balanced angle-ply graphite/epoxy specimen carefully to get accurate values of specimen strains. It can be observed from the results shown in Figure 15 that the strain values obtained from the bar and the actual strain in the specimen agree well up to the maximum strain values.

The time lag for the transmitted wave compared to the reflected wave can be used to interpret the results of the SHPB test. The homogenization time for all balanced angle-ply graphite/epoxy specimens is lower than the corresponding time of failure as shown in Table 4. The term γ represents the number of times the pulse reflected back and forth to produce uniform stress in the specimen. The value of γ for graphite/epoxy system is four [9]. In other words, the purpose of these reflections is to ensure the specimen is in equilibrium at failure and check the

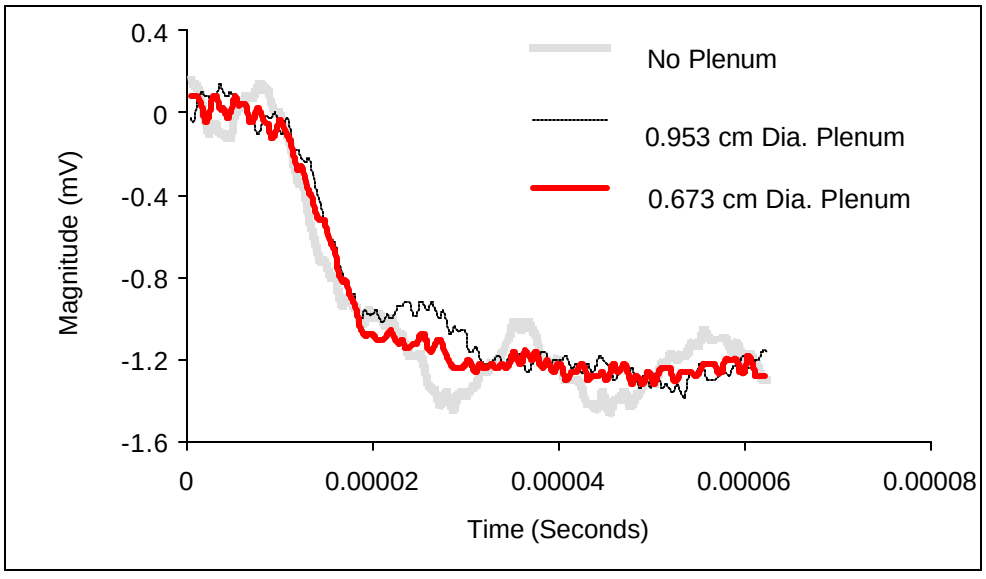

Figure 13 Plenum size impact on pulse shape.

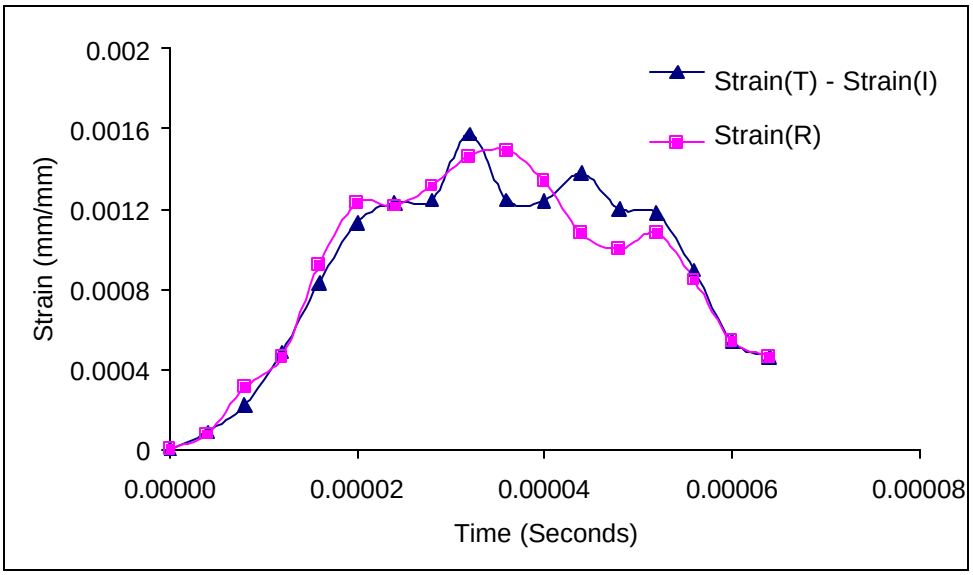

Figure 14 Verification of equation of dynamic equilibrium.

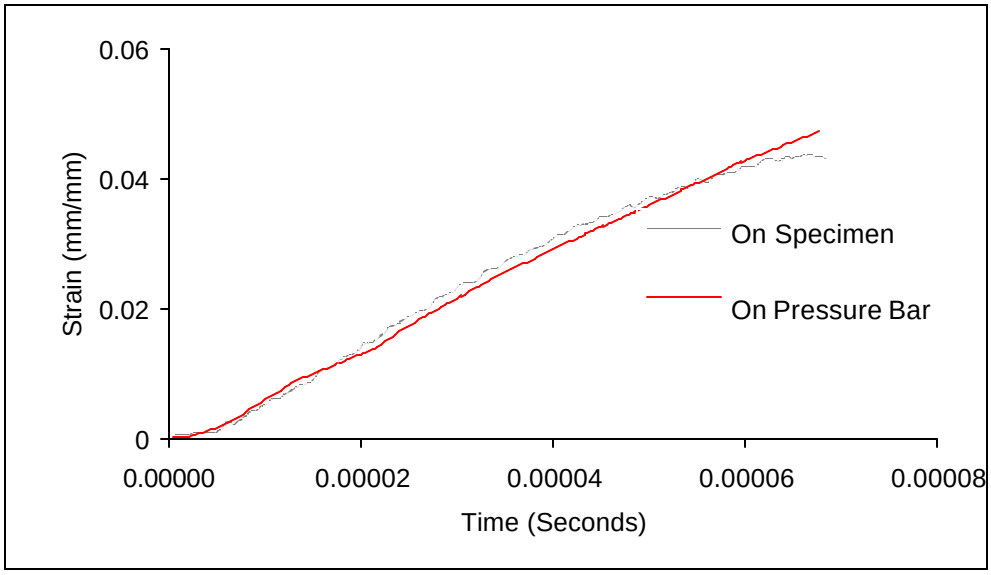

Figure 15 Comparison of strain values obtained by direct strain measurement using a graphite/epoxy specimen and by using SHPB.

validity of the tests. The transient time, t_s, is obtained by measuring the time gap between the transmitted and reflected waves. This time represents the delay in the transmitted wave due to the time required for it to travel through the specimen. In the absence of a specimen, both transmitted and reflected waves should be coincident due to the strain gauge placement at the

same distance on the pressure bars. The time to failure is obtained from experiment. The minimum time to failure is therefore $\gamma * t_s$, and is the total time required for the specimen to be intact, at which time the wave reflects back and forth so that the uniform stress assumption remains valid.

Table 4 Time to failure for the off-axis graphite/epoxy specimens.

Specimen off-axis orientation (Degrees)	Transient time t_s (μs)	Minimum time to failure $\gamma * t_s$ (μs)	Time to failure t_f (μs)
15	8	32	37
30	4	16	18
45	12	48	57
60	8	32	57
75	10	40	59

4 RESULTS AND DISCUSSION

4.1 High Strain Rate Properties of Balanced Angle-Ply Graphite/Epoxy Composites

4.1.1 Quasi-Static Tests

The strain rates of about $0.001s^{-1}$ are obtained using MTS servo-hydraulic machine. The axial ultimate engineering stress and initial modulus are found to be decreasing with increasing angle. The decrease in modulus for 15^o and 30^o is found to be less than 5% as compared to the 0^o off-axis (longitudinal) specimens. The elastic modulus values are minimum for 90^o off-axis fiber orientation (transverse direction) where the properties are controlled by the matrix rather than the fibers. The ultimate stress range for 45^o, 60^o and 75^o fiber orientation specimens is found to be narrow. However, the 45^o specimens show high axial strain (0.105 mm/mm) due to the fact that there is no lateral constrains placed while testing. The dominant failure mode observed is delamination. The presence of interlaminar shear stress caused by edge effects is expected to be the probable cause for the delamination. The ultimate axial strength values for various fiber orientations are plotted in Figure 16. These values are similar to published results in the literature [28].

4.1.2 High Strain Rate Tests

4.1.2.1 Stress-Strain Behavior and Strain Rate

One of the important aspects of this study is to compare the stress versus strain behavior of various fiber orientations of balanced angle-ply laminates at the same strain rate. Typical dynamic stress versus strain curves for specimens having different fiber orientations tested at

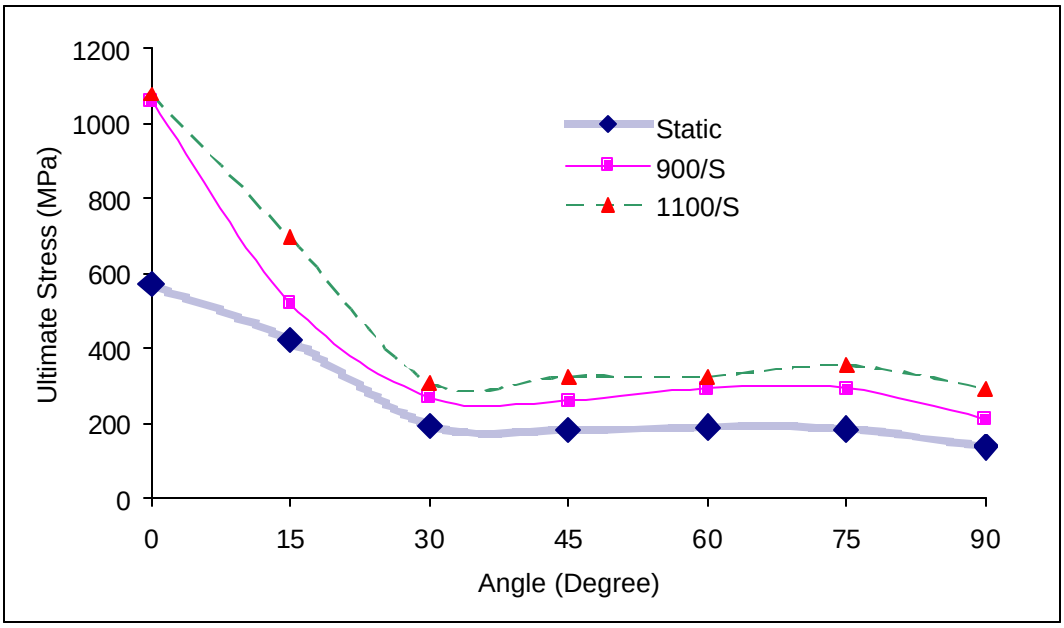

Figure 16 Orientation dependence of maximum stress at various strain rates.

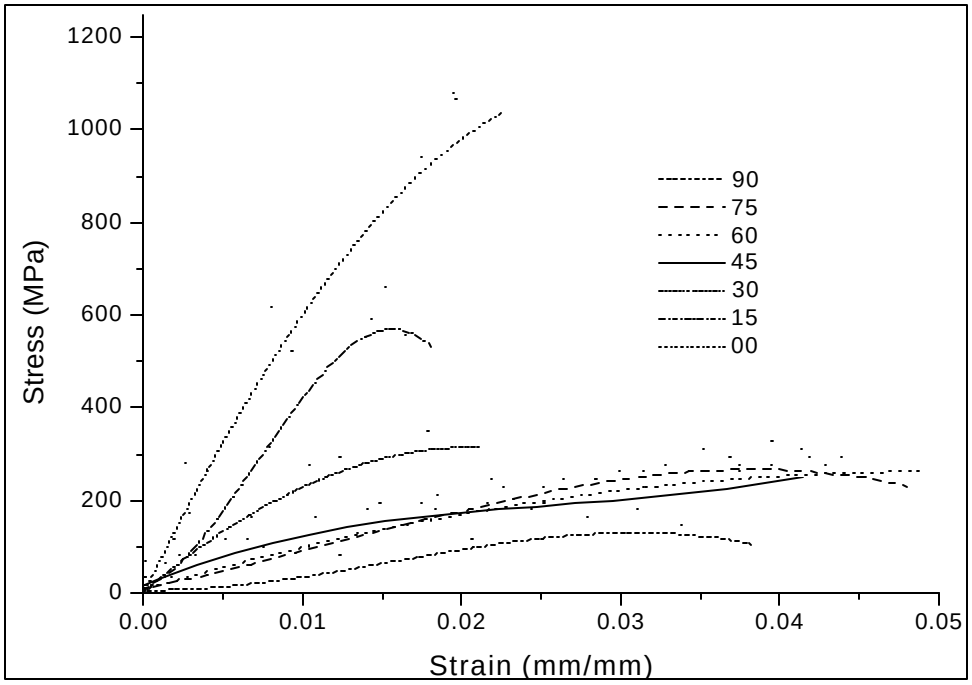

Figure 17 Axial Stress vs. Axial Strain for several fiber orientations at strain rates of around 1050/ s.

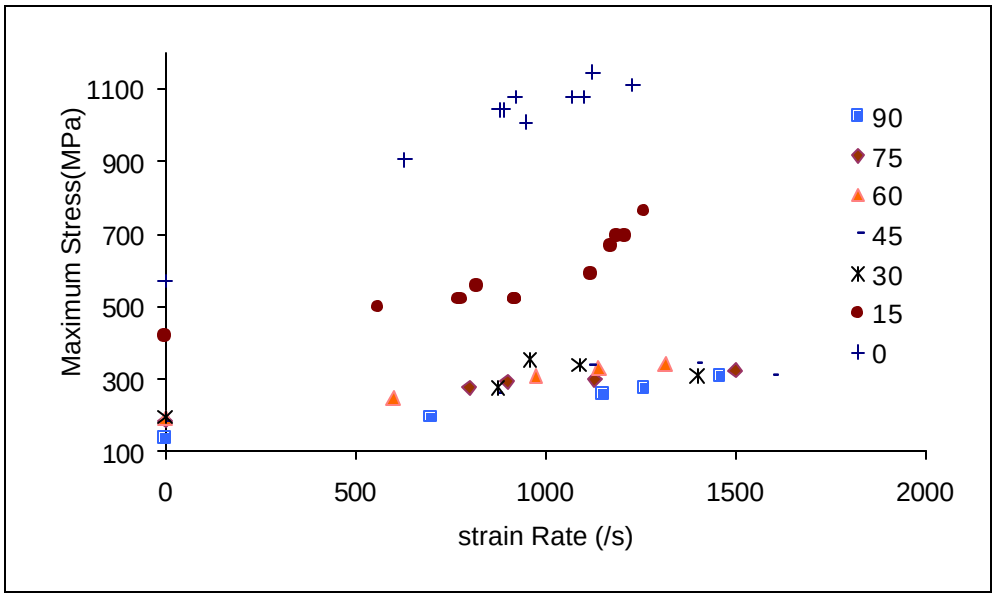

Figure 18 Ultimate Stress values for various fiber orientations at different strain rates.

strain rates of around 1050 /s is shown in Figure 17. The ultimate stress value is seen to be decreasing uniformly as the fiber orientation angle increases. The summary of results for various balanced angle-ply laminate specimens is shown in Figure 18. From this figure, the significance of strain rate variation on the ultimate strength properties of various fiber orientations for balanced angle-ply laminates can be observed clearly. For all fiber orientations, the ultimate stress value increases as the strain rate increases. This can be attributed to the fact that at slower strain rates the damage propagates more slowly utilizing most of the applied energy. However, at higher strain rates, the damage doesn't have enough time to initiate and propagate, and thus a higher amount of energy is absorbed under this situation. For the increase in ultimate strength of the specimens tested in transverse direction at high strain rates, the viscoelastic nature of the polymer matrix itself is responsible in addition to the time dependent nature of accumulating damage [34]. The high strain rate ultimate strength values at orientations of $\pm 30^{o}$ and above are close to each other as they are for quasi-static ultimate strength values for similar orientations. The main reason for this occurrence is the matrix domination in determining the properties of the

composites with increasing fiber orientation. It can be inferred from Figure 18 that the strain rate sensitivity of the material is prominently high at relatively low (static to 200 s^{-1}) strain rates. Figure 16 also shows the compressive ultimate strength at different fiber orientation angles for high strain rates. It can be seen that the difference in maximum strength between static and dynamic tests decreases as orientation of fibers increases. The mode of failure of fiber-reinforced composites is the determining factor of the strain rate sensitivity magnitude. This observation explains why the strain rate effect on ultimate stress is more pronounced with decreasing fiber orientation. There is no sudden drop in the ultimate stress and strain values at $\pm 60^o$ angle laminates, which is contrary to the previous study done by Vinson and Woldesenbet [35] for unidirectional off-axis laminates of graphite-epoxy. The probable cause of failure was given that the 60^o plane could be the plane of maximum dynamic shear stress due to shear coupling. This coupling of in-plane shear stresses is avoided in the case of balanced angle-ply laminates for the same fiber orientation. Instead, delamination failure caused by the edge effect is a prominent mechanism of failure in case of these laminates.

Figure 19 shows the change in the ultimate compressive strain as a function of strain rate for three different orientations. It is observed that the ultimate strain values for 0^o and $\pm 15^o$ samples are least affected by the change in strain rates. The $\pm 45^o$ and $\pm 60^o$ are found to have undergone maximum amount of strain. Most of the $\pm 30^o$ samples showed relatively less failure strains in high strain rate testing with a high amount of scatter in values. The highest fracture strain is obtained under quasi-static loading conditions. However, in the dynamic region, the fracture strain is very low (almost 30-40% of static values) for lower strain rates (500 s^{-1}). It increases as the strain rate is increased. A sharp increase in fracture the strain values is noted for almost all fiber orientations at strain rates ranging from 800 to 1100 s^{-1}.

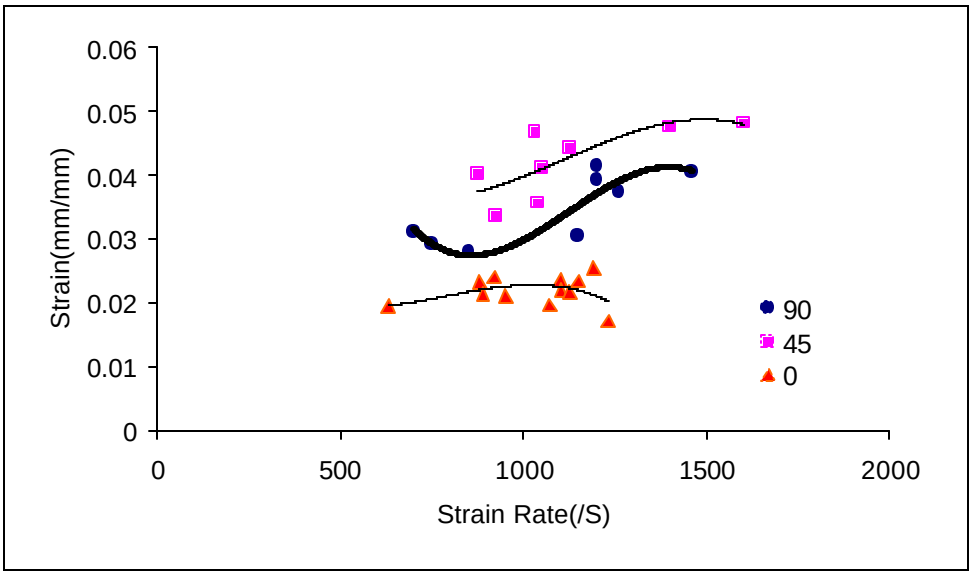

Figure 19 Ultimate strain values for various fiber orientations at different strain rates.

4.1.2.2 Effect of Strain Rate on Modulus

It has been found by a number of researchers [31-32, 35-36] that the strain measurement and therefore modulus determination is difficult by the SHPB and the acquired data is not very reliable. However, in general, it is observed that the high strain rate modulus values are approximately threefold in longitudinal direction compared to static values. Also an appreciable increase in the transverse modulus is observed at high strain rates. These values are mentioned in Table 5. Figure 20 shows compressive stress-strain curves for $[\pm 15^{o}]_{s}$ specimens tested at different strain rates. As compared to the static stress-strain curve, significant stiffening of the stress-strain curves can be observed at higher strain rates due to viscoelastic nature of polymer matrix. Similar trends are observed for other fiber orientations as well as exhibiting increased initial modulus with increasing strain rates. Also, large amount of scatter in the modulus values is observed in the range of 1000 s^{-1} to 1500 s^{-1}. It was observed from the shape of the stress-strain curves that the amount of non-linearity in the curve increases as the fiber orientation increases from its longitudinal direction to $\pm$ 45 degrees.

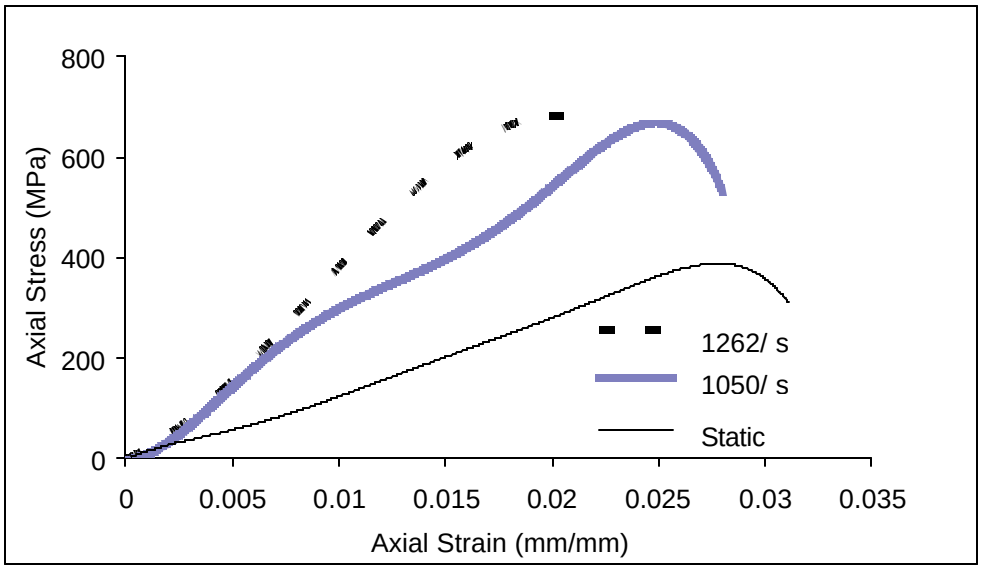

Figure 20 Static and dynamic stress-strain curves for $[\pm 15^{o}]_{s}$ specimens.

Table 5 Longitudinal and transverse modulus values of unidirectional IM7/8551-7 graphite/epoxy composites at various strain rates.

Strain Rate (s^{-1})	Modulus E_1, GPa	Percentage Change	Strain Rate (s^{-1})	Modulus E_2, GPa	Percentage Change
0.001	26.66	-------	0.001	5.28	-------
630	62.14	133.08	800	7.10	34.46
920	77.77	191.71	1140	7.61	44.12
1100	81.00	203.30	1400	8.37	58.52

4.1.3 Modes of Failure

Specimens subjected to static compression loading in the longitudinal direction are mainly found to undergo transverse tensile failure and fiber microbuckling. This could occur when the transverse tensile strains resulting from the Poisson's ratio effect exceed the ultimate transverse strain capability of the specimen. The high strain rate failure mechanism for longitudinal fiber orientation specimens mainly consists of delamination including longitudinal matrix cracking and fiber micro buckling. The phenomenon of micro buckling become clear

from Figure 21. A micro-buckled layer of bunch of fibers can be observed where load is applied along the fiber orientation. Also delamination is very common at excessively high strain rates as shown in Figure 22. Figure 23 shows the optical microscopic image of a high strain rate longitudinal specimen that fails in matrix breaking. Similar kind of failure mechanism is seen in the case of 15 degree balanced angle ply laminates. Here, damage is initiated by matrix cracking; when a matrix crack reaches an interface between layers with different fiber orientations, delamination occurs. Delamination is the primary mode of failure for quasi-static as well as high strain rate testing. The $\pm 30^{o}$, $\pm 60^{o}$ and $\pm 75^{o}$ samples show the mixed modes of failure in shear as well as delamination for quasi-static rates.

The $\pm 30^{o}$ fiber orientation sample prominently show more shear failure than the delamination. Figure 24 shows a 30^{o} specimen undergoing complete shear type of failure with relatively less values of peak stress and total strain. The introduction of shear failure may be caused by the initiation of failure due to delamination and subsequent in-plane shear stress failure of individual lamina. The shear plane is found to cut through the fibers for some samples. In the cases of shear failure, two shear bands usually join together and form a delamination site.

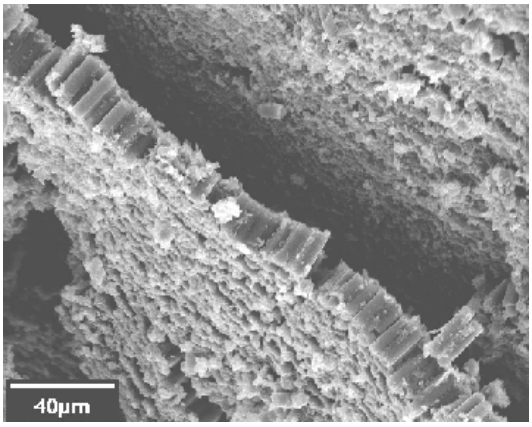

Figure 21 Specimen loaded longitudinally under dynamic conditions fails in microbuckling.

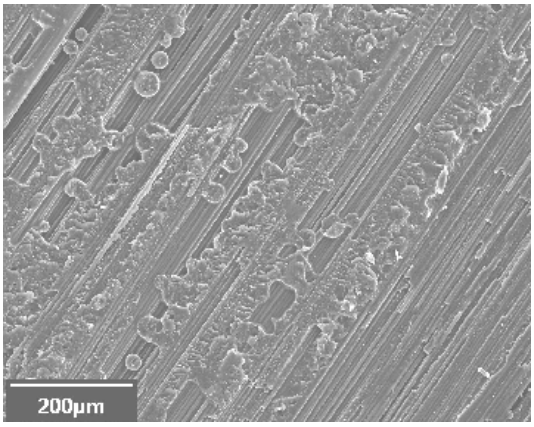

Figure 22 HSR longitudinally loaded specimens fail in delamination.

In dynamic testing of $\pm 60^{o}$ and $\pm 75^{o}$ specimens, typically delaminated fractured surfaces joined by some jumps of sheared surfaces are observed at lower magnifications as shown in Figure 25. Being a balanced angle-ply laminate, the delamination initiates at the surface of the specimen, which continues further into of the specimen and tends to fail the specimen in shear. A typical delaminated portion of such a specimen is shown in Figure 26. Delamination caused by debonding of fiber-matrix interfaces and matrix breaking are visible. The shining and clear portion of fibers shows the debonding. The central portion, which goes under considerable shear

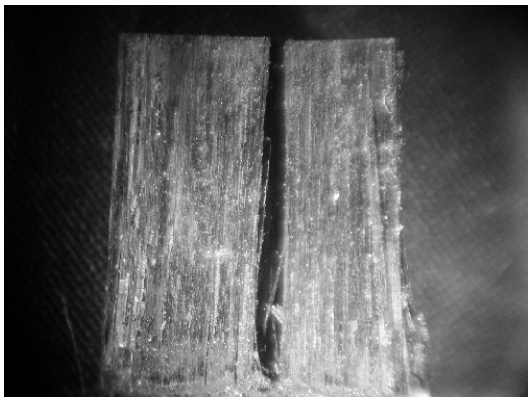

Figure 23 Vertical splitting of a 0^{o} specimen under high strain rate loading.

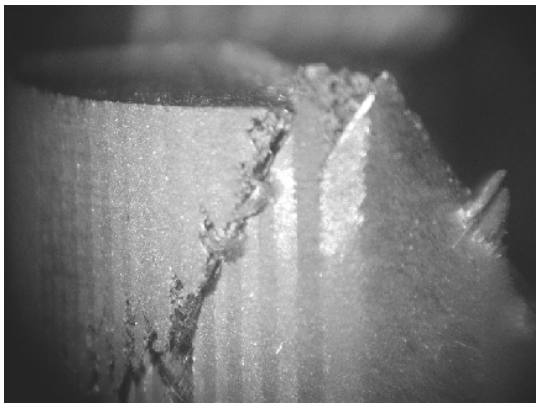

Figure 24 Complete shear type of failure for a $[\pm 30^{o}]_{s}$ specimen.

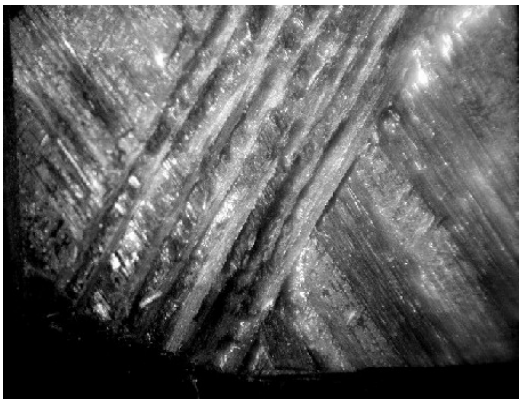

Figure 25 A $[\pm 60^{o}]_{s}$ specimen loaded under dynamic conditions.

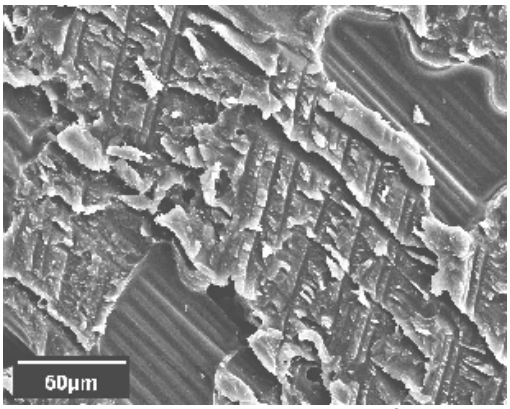

Figure 26 Delamination for a $[\pm 75^{o}]_{s}$ specimen.

propagates along -θ direction breaking all the +θ fibers in shear. The fibers are clearly shown to fail in shear with somewhat ductile manner in Figure 28. The fibers along the -θ remain unbroken. A SEM micrograph along that layer shows fiber pullout, Figure 29. Considerable river marks are also evident from this figure, which show the direction of crack propagation in the matrix.

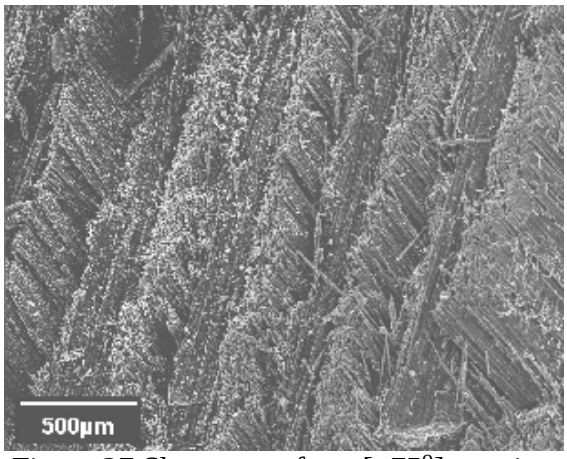

Figure 27 Shear steps for a $[\pm 75^{o}]_{s}$ specimen.

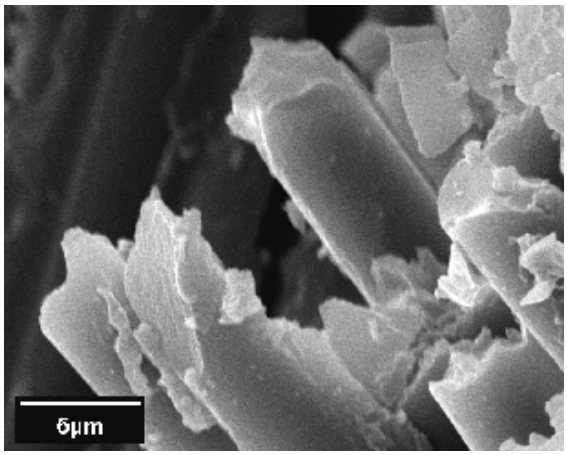

Figure 28 SEM image of 'ductile' failure for a $[\pm 75^{o}]_{s}$ specimen.

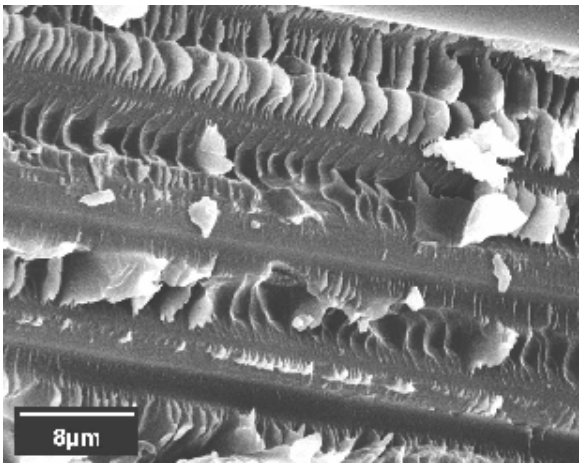

Figure 29 Considerable fiber pull-out and river marks along -θ direction in case of a $[\pm 75^{o}]_{s}$ specimen

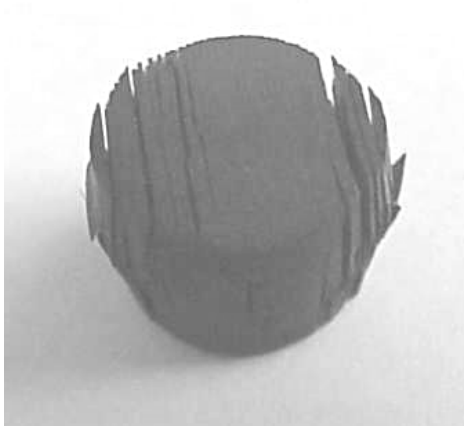

Figure 30 A $[\pm 45^{o}]_{s}$ specimen showing total delamination.

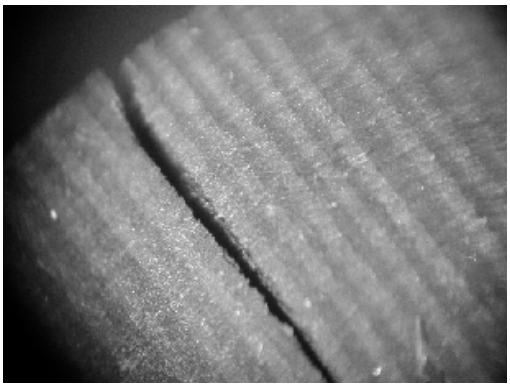

Figure 31 Delamination plane traveling along a vertical plane under high strain rate conditions for a $[\pm 45^{o}]_{s}$ specimen.

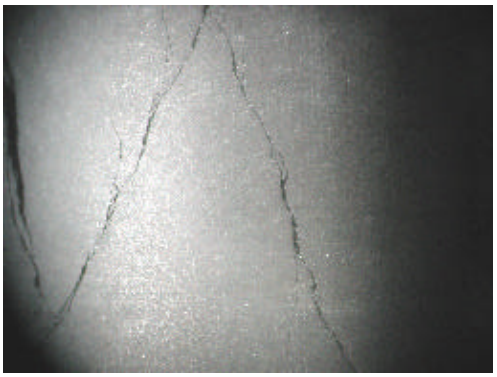

Figure 32 Optical Micrograph of fracture surface of a transversely loaded specimen under static loading.

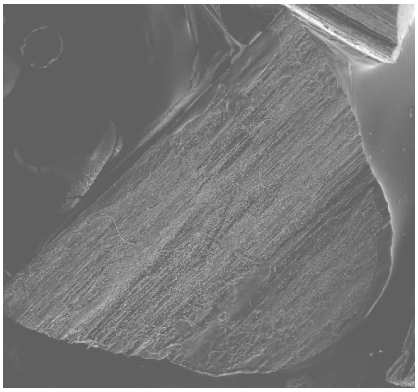

Figure 33 Top view of fracture surface of a transversely loaded.

For all 45^{o} balanced angle-ply laminate specimens, total delamination is observed. Figure 30 shows the optical micrograph of a delaminated specimen under quasi-static conditions. The delamination caused by interlaminar shear stresses is developed due to edge effects. The shear mode of failure is totally absent in both cases of static and dynamic loading. This confirms the decoupling of in-plane shear in balanced angle ply laminates. This observation is clearly shown in Figure 31, which shows the crack initiations and propagation along the interface of two laminas. For transversely loaded specimens (90^{o}), matrix shear failure is seen to be dominant as suggested by Collings [37]. Under static compressive loads, shear failure occurs on 45^{o} plane,

Figure 32. The shear mode changes to delamination when the applied stress and strain rates are increased. Top view of another specimen failed in shear under dynamic loading conditions is as shown in Figure 33. Vast matrix breaking is observed at higher magnifications.

4.2 High Strain Rate Properties of Syntactic Foam and Density Effects

4.2.1 Stress-strain Behavior

High strain rate compression test results of four types syntactic foams are discussed here to establish the effect of strain rate and effect of syntactic foam density on the dynamic compressive properties of syntactic foams. The results at high strain rates are compared to quasi-static strain rate compressive properties of the same material. Typical engineering stress versus engineering strain curves for various foam densities obtained at strain rates around 1050 s^{-1} are shown in Figure 34. An almost linear initial region is found for each stress-strain curve where stress is directly proportional to strain up to about 3% strain. Another general observation for each of them is that when the compressive strain is between 3.5 to 4%, the stress reaches its peak value. The foam density is not found to influence the strain at peak stress. This fact strongly indicates that the critical strain at which peak strength is observed does not depend on the type of cenospheres and can be primarily recognized as the matrix property. Contrary to quasi-static stress-strain curves in high strain rate experiment, the stress values don't drop drastically after maximum stress. Only a small decrease in stress is observed after the peak stress value. After the peak, the stress stays nearly constant for increasing strain until it drops suddenly corresponding to the ultimate failure of the specimen. For some of the lower density specimens tested under dynamic conditions, stress oscillations are observed in this constant stress region, which indicate the fracture front propagation through specimen length. A constant stress region, called the plateau region, is also observed in the quasi-static test results, which is termed as the

densification stage. The main reason for the densification stage in the quasi-static tests is the fracture of cenospheres. Compressing material consumes the space of cenospheres and increases the overall density of the syntactic foam. Microscopic evidences will be sought in the later sections to determine if the same kind of phenomena occurs in high strain rate tests.

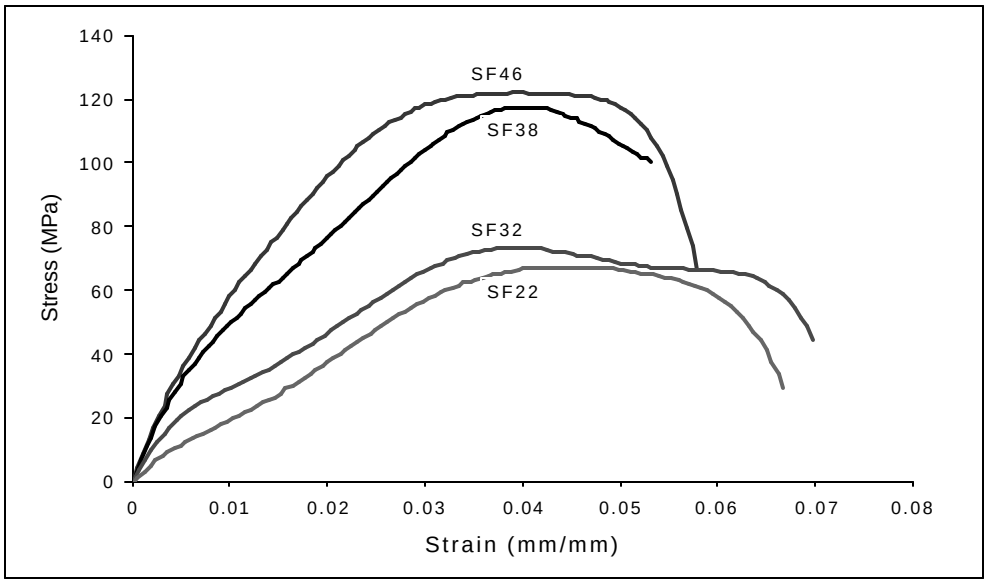

Figure 34 Stress vs. Strain for various densities of syntactic foam at strain rates of around 1050 s^{-1}

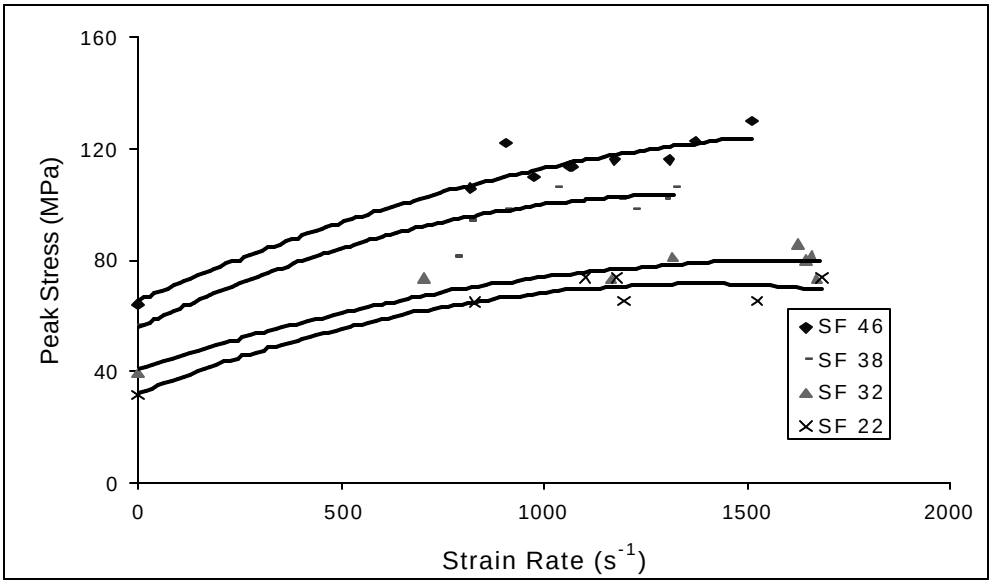

Figure 35 Peak Stress values for various syntactic foam densities at different strain rates.

The strain rate dependence of peak stress for various types of foams can also be observed in Figure 35. Almost twofold increase in peak stress values is attained at the strain rates of about 1700 s^{-1} compared to quasi-static value in all types of syntactic foams. The increase in maximum strength with increase in strain rate can be attributed to the fact that at slower strain rates, the damage propagates more slowly expending most of the applied energy. However, at higher strain rates, the damage doesn't have enough time to propagate, and thus a higher amount of energy is absorbed under this situation. This is accomplished by increase in stress level as compared to quasi-static conditions for similar strain values. Additionally, viscoelastic nature of the polymer matrix itself is responsible in addition to the time dependent nature of damage accumulation. Another observation from Figure 35 indicates that similar to quasi-static testing, the maximum stress values increase with increasing the syntactic foam density in high strain rate tests. The peak stress is calculated to be 130.8 MPa for the SF46 foam having density value of 460 kg/m^3 and progressively decreases with decrease in density and becomes about 65.4 MPa for SF22 syntactic foam having density value of 205 kg/m^3.

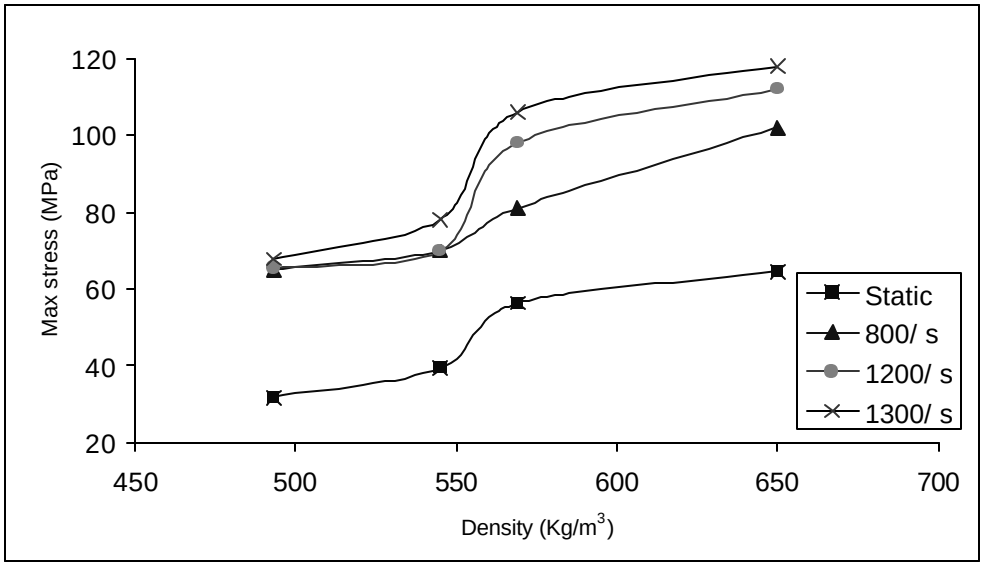

Figure 36 Syntactic foam density dependence of maximum stress at various strain rates.

It is possible to consider the combined effect of strain rate and density of the syntactic foam on peak stress values in different strain rate ranges. Figure 35 shows almost linear increase in peak stress values with increasing strain rates for higher density syntactic foams (SF46 and SF38). For lower density foams, this increase is linear up to the strain rates of about 1100 s^{-1} and then it becomes nonlinear where the curves become almost flat. This phenomenon is more apparent from Figure 36 where with increasing strain rate, lower density foams show relatively less increase in peak stress values compared to those of higher density foams. This means that in case of the lower density (higher η) foams, the strain rate sensitivity of peak stress decreases at higher strain rate values where cenospheres play major role in sustaining applied stress. At lower strain rates where matrix failure is more dominant, the peak stress values appear to be almost equally strain rate sensitive regardless of the density of the foam. The variation in strain rate sensitivity of the syntactic foams in different strain rate regions will become clear in the section on failure mechanisms of foams where it can be found out that the mode of failure is the determining factor for strain rate sensitivity.

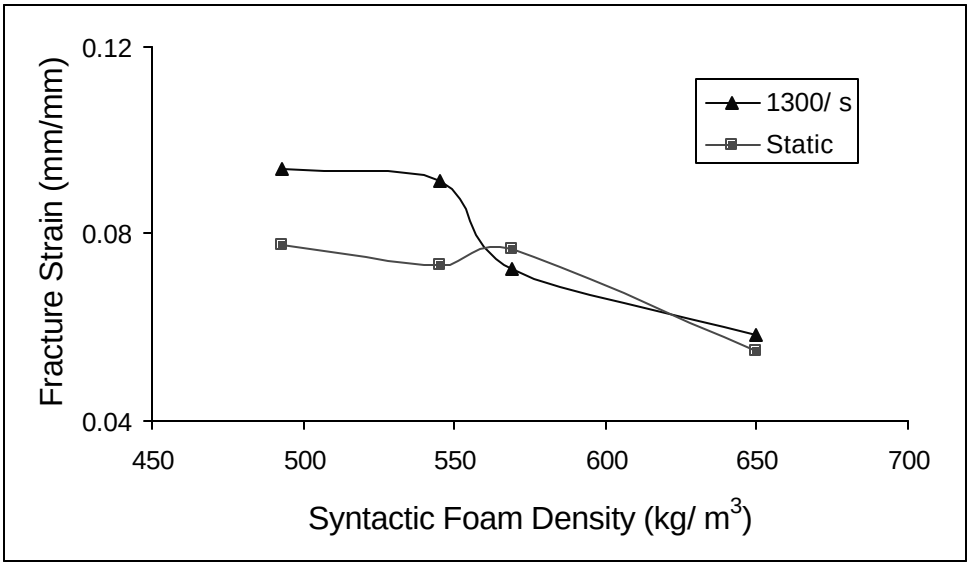

Figure 37 Fracture strain values for various foam densities at different strain rates.

Crushing of cenospheres is a considerably important mechanism of failure for lower density syntactic foams under quasi-static conditions of loading. Considerably high failure strains can be expected in this case due to the availability of newly created space due to the breaking of hollow cenospheres. With increase in density of syntactic foam, vertical cracks originated under lateral secondary tensile stresses limit the total strain in the materials before its failure. In this case lower failure strain can be expected. These phenomena are quite clear from Figure 37. It can be observed that under quasi-static loading, the failure strain decreases considerably from 9.41% for SF22 to 5.82% for SF46. The failure strain remains almost the same at high strain rate (~1300 s^{-1}) for higher density syntactic foams but the gap between failure strains at quasi-static and high strain rate increases considerably at lower densities of the foam. Thus it is clear that under dynamic conditions of loading, even lower density foams are more susceptible to vertical cracking of the materials than crushing of cenospheres. In general increasing trend of failure strain with decreasing density of the syntactic foam becomes less and less prevalent with increased strain rates.

4.2.2 Effect of Strain Rate on Modulus Values of Syntactic Foams

Figure 38 shows stress-strain curves for SF38 syntactic foam at various strain rates. It can be observed that stress-strain curves get stiffened significantly at higher strain rates compared to the static curve due to the viscoelastic nature of the polymer matrix. Similar trends are observed for all types of foams. Compressive modulus values for all types of foams at various strain rates are presented in Table 6. An appreciable amount of increase in modulus values is observed for all kind foams with increase in strain rate. At the strain rates of about 1700 s^{-1} up to 37% increase has been noted in the modulus as compared to quasi-static value. It is interesting to note here two facts. First, the volume fraction of the polymer matrix is the same for each type of foam. Second,

for all types of foams the percentage changes in the elastic modulus values at any similar higher strain rates compared to the respective quasi-static values are almost the same. Hence, it can be concluded that elastic modulus variation is due to the matrix part of foam only and not due to cenospheres.

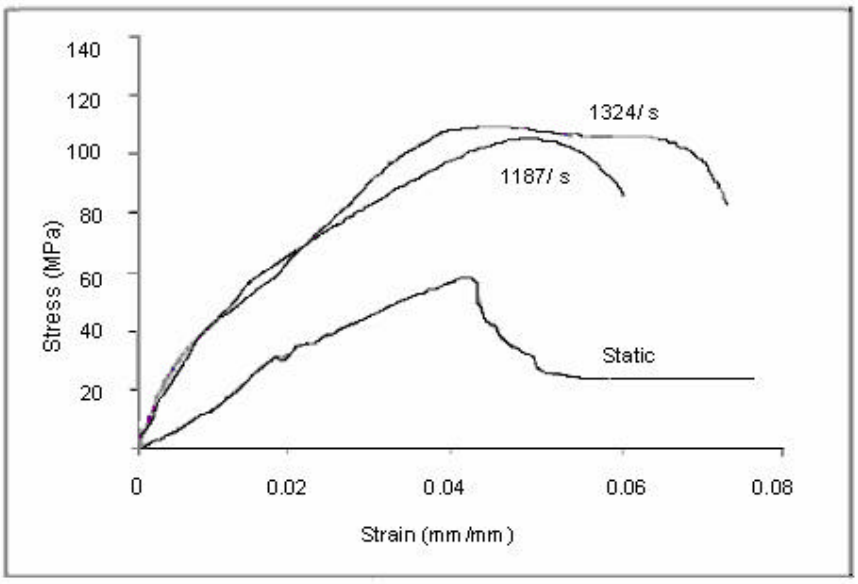

Figure 38 Static and dynamic stress-strain curves for SF 38 specimens.

Table 6 Change in modulus of syntactic foams with strain rate.

Syntactic Foam Type	Strain Rate (s^{-1})	Modulus E (MPa)	Percentage Change
SF 22	Static	1547	-
	830	1777	14.86
	1200	1969	27.77
	1688	2503	37.29
SF 32	Static	2025	-
	703	2191	8.19
	1164	2372	17.13
	1636	2601	28.44
SF 38	Static	2394	-
	830	2796	16.79
	1030	2888	20.63
	1324	2864	19.65
SF 46	Static	2639	-
	979	3132	18.68
	1015	3161	19.78
	1460	3564	35.20

4.2.3 Energy Absorption

Energy absorption in syntactic foams is due to various sources such as cenosphere fracture, elastic and plastic deformation of polymeric matrix and matrix-cenosphere interfacial fracture. Additionally, friction in relative and rotational movement of the broken pieces of cenospheres during deformation process consumes energy. The energy absorbed per unit volume by a material can be given by the area under the stress-strain curve and can be expressed by Equation 30.

$$C = \int_0^l s\,de \tag{30}$$

where s is compressive stress, l the limit of strain concerned, and e strain. The areas under the stress strain curve up to 5% strain were calculated, as it is the maximum strain obtainable at the lowest strain rate in SHPB.

Figure 39, compares the energy absorbed by syntactic foams at various strain rates as a function of foam density. It can be noted that the data trend in this graph is similar to that in Figure 36. With increase in the strain rate, the energy absorption capacity per unit volume of the foam is found to be increasing. This is because stress level increases with strain rate; hence at any given strain value the area under stress-strain curve increases considerably. Also higher density foams are much more efficient in energy absorption as compared to lower density ones. In all the above cases, increase in energy absorption capability in the elastic range is due to increase in elastic modulus with strain rate. A low elasticity modulus implies a low stress wave speed C, at which stress wave (and the accompanying strain energy) propagates from the point of impact. The wave speed C is related to material's elasticity modulus E and its density r by Equation 2 in chapter 2. Hence the amount of strain energy that foam can absorb is also

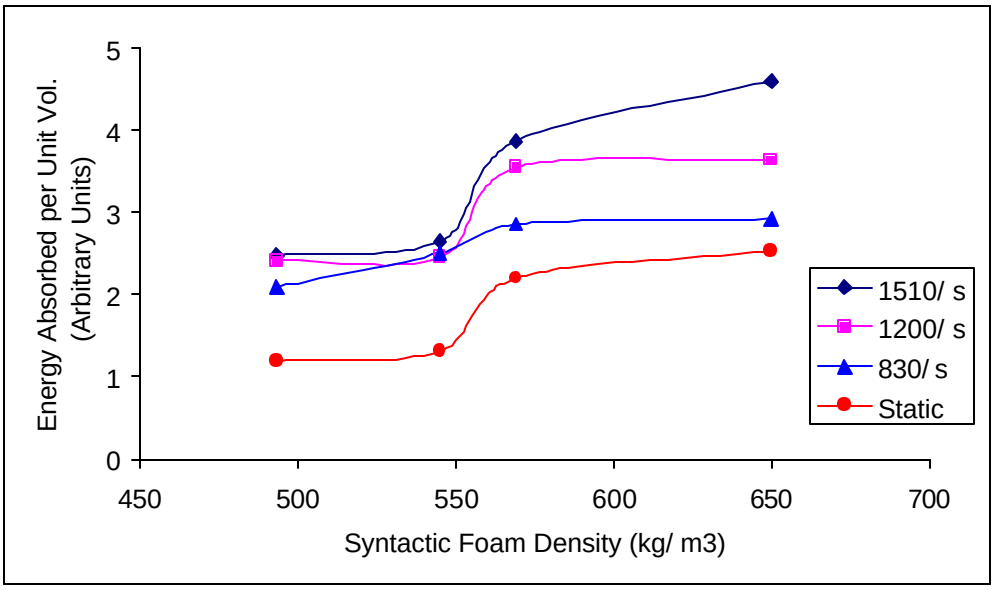

Figure 39 Energy absorbed per unit volume as function of syntactic foam density and strain rate.

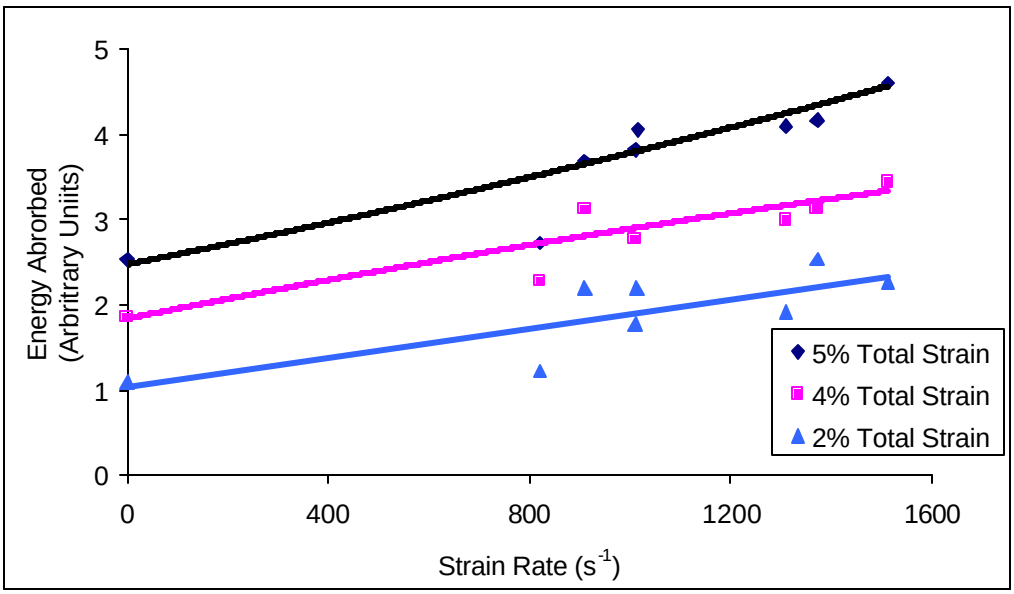

Figure 40 Energy absorbed per unit volume at three different strain values for SF46 specimens with increasing strain rates.

dependent on its modulus of elasticity. With increase in the modulus, there will be an increase in dispersion of localized caused by impact. Thus the amount of energy absorbed by the foam is expected to increase with modulus of elasticity.

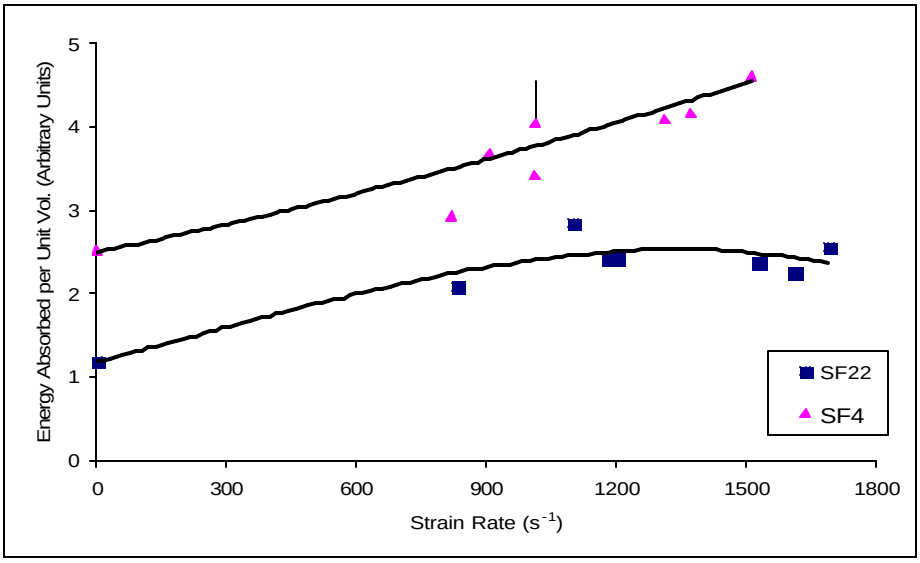

Figure 41 Comparison of Energy absorbed per unit volume by SF 46 and SF22 with variation in strain rates.

Figure 40 shows that for SF46 syntactic foam, increase in energy absorbed per unit volume as a function of strain rate increases linearly for three different strain values of the material. Figure 41 shows the energy absorbed by SF22 and SF46 at different strain rates. No significant increase in energy absorption per unit volume for SF22 foam is observed in the strain rate range 830 s^{-1} to 1510 s^{-1}. It appears to be close to saturation in that limit. On the contrary, for the SF46 foam the energy absorbed increases almost linearly with linear increase in strain rate in the range of high strain rate testing. Hence, it can be concluded that the energy absorption capacity is highly strain rate sensitive. Impact at high strain rate causes the crack to propagate through the cenospheres. This makes higher density syntactic foams (containing thicker walled cenospheres) difficult to break and absorb more energy than thinner walled cenospheres such as SF22. Hemispherical failure of cenospheres, which is a typical characteristic of high strain rate failure mechanism, controls the energy absorption. On the contrary to this case, energy absorption character is controlled by matrix and interface failures along with shear failure at

lower strain rate values. At high strain rates, breaking of cenospheres becomes more difficult in case of higher density foams compared to lower density foams

4.2.4 Modes of Failure

In the quasi-static compression tests of syntactic foams it is observed that the specimen failure takes place under the combined effects of shear and secondary tensile stresses as shown in Figure 42. Specimen of SF38 syntactic foam is shown in this figure. Shear cracks originate from the corners of the specimens and propagate at 40-60° angles. Cracks originated under lateral secondary tensile stress are in the direction of applied load. It is noticed that as the foam density increases, vertical splitting becomes more and more prominent. Also initiation of the crack is highly influenced by the stiffness of the material. Higher stiffness syntactic foams, with lower cenosphere η, show early formation of the vertical crack. On the contrary, the foams with higher cenospheres η show higher strains before origination of vertical crack and also the final failure of the specimen. The higher specimen failure strain also leads to more crushing of cenospheres in the syntactic foams.

Failure modes of specimens tested at high strain rate are evaluated using optical and scanning electron microscopy. Although the stress-strain responses of the individual category of syntactic foam specimen portray some unique characteristics, the foam samples share some common modes of failure for all kind of foams.

In high strain rate test specimens crack starts from one end and propagates to the other end through the specimen cross section. It initiates with two shear planes from the same end, which eventually join together and form a crack plane. Substantial amount of damage is noticed on the crack places because of crushing of cenospheres as shown in Figure 43. Debris of cenospheres is visible all over the micrographs in this figure. Optical micrograph of two shear planes originated

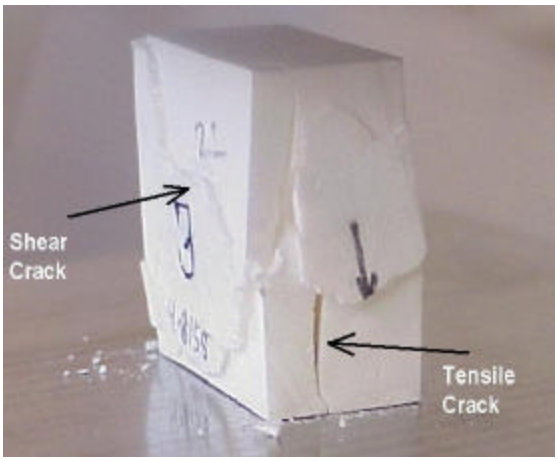

Figure 42 A SF38 syntactic foam specimen failed in mixed failure in shear and vertical splitting.

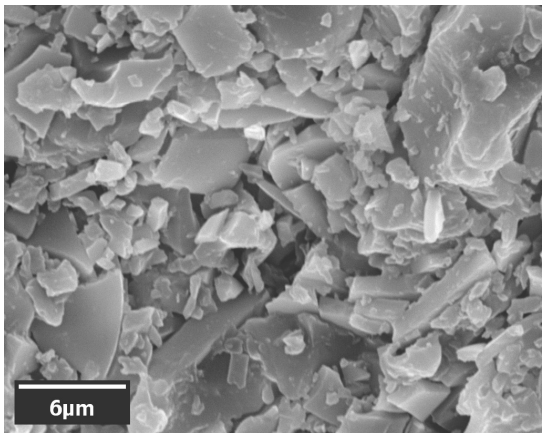

Figure 43 Debris of crushed cenospheres at the end of a specimen.

at the specimen that join together is shown in Figure 44. At the point where the shear cracks meet, a new crack originates under the effect of secondary tensile stresses. This crack then travels through the specimen causing the ultimate fracture. The higher the strain rate, the lower will be the shear failure at the ends and most of the fracture will be a result of straight cleavage like tensile crack plane. A typical example of this kind of fracture is shown in Figure 45, which shows an SF46 specimen tested at 1680 s^{-1} strain rate. In this figure a straight crack plane is initiated at the incident end of the specimen, which eventually propagates to the transmitted end without any deviation.

The failure mechanisms seem to be similar in both low and high strain rate-testing cases with only difference being in the extent of shear failure zone. However, scanning electronic micrographic observations reveal some interesting differences. In the lower strain rate test specimens it is observed that the crack propagates through either the matrix material or the matrix-cenosphere interface as shown in Figure 46. Crack does not tend to fracture cenosphere and bypasses them completely. In higher strain rate test specimens, crack tends to fracture the cenospheres while propagating as shown in Figure 47. A higher magnification micrograph shows

the crack propagation and the fracture of a cenosphere in Figure 48. This makes the consumption of more amount of energy at high strain rates and requires higher amount of stresses for fracture as compared to quasi-static testing. Figure 49 shows the side view of a failed specimen under dynamic loading. Here, like a typical brittle like fracture, the fracture plane passing through cenospheres and produces hollow hemispheres.

In many cases, a network of cracks derived from the original crack plane or from either of the specimen ends or from voids was observed. The voids in the specimen are also found to be "attraction centers" for the cracks and cause fracture planes to change their original direction.

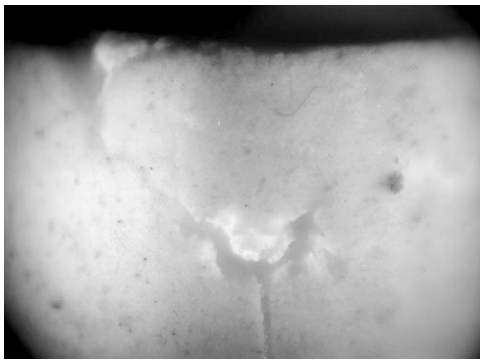

Figure 44 Shear planes originated at the specimen end join later to form a vertical crack.

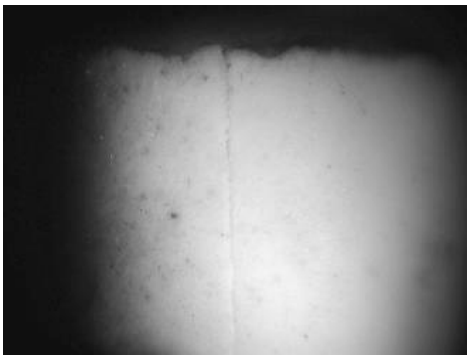

Figure 45 Crack originated at the specimen end causing vertical splitting in the specimen.

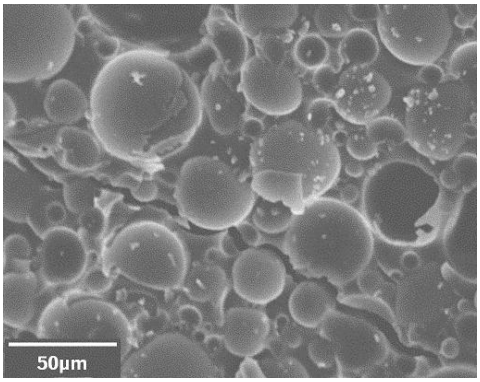

Figure 46 A low strain rate crack avoids cenospheres.

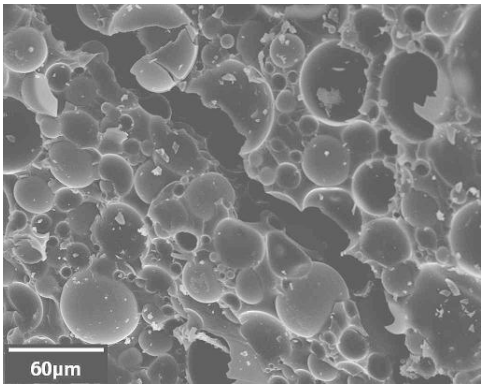

Figure 47 Crack passing through cenospheres under HSR condition.

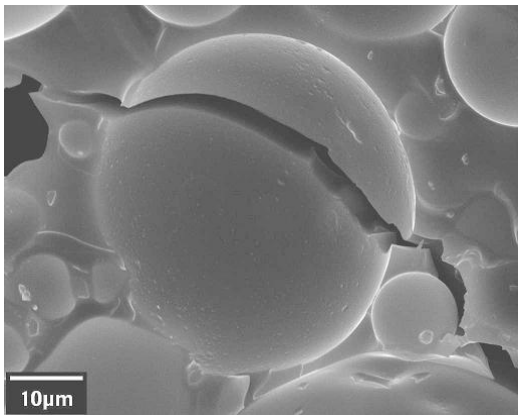

Figure 48 Enlarged view of figure 47 showing crack's path through a cenosphere.

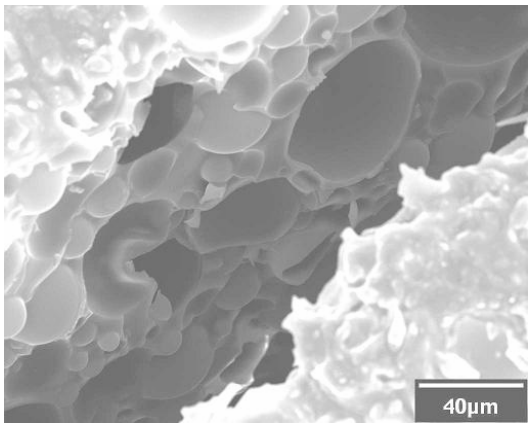

Figure 49 Crack plane passing through cenospheres.

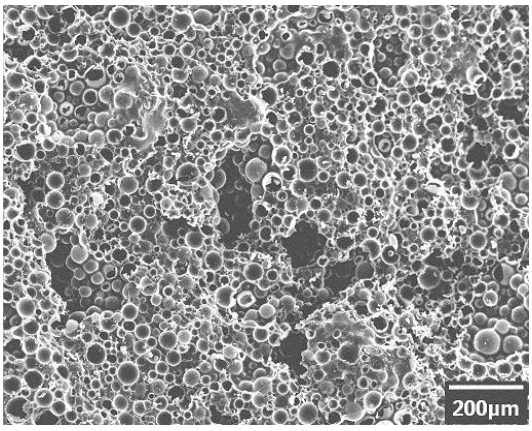

Figure 50 Crack planes observed to be attracted by higher void density.

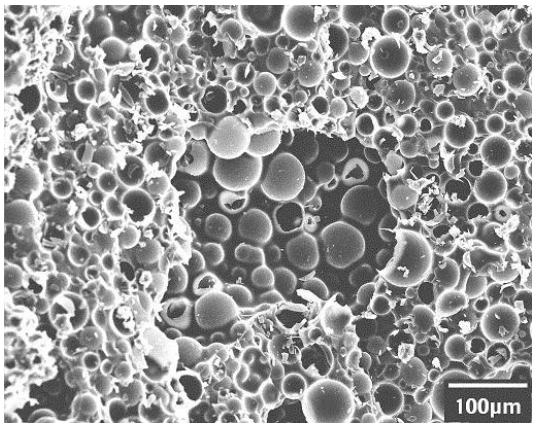

Figure 51 Fracture surfaces meeting at a void.

Figure 50 shows an SEM image of fracture planes meeting at a void site. Another SEM image (Figure 51) shows a fracture plane being attracted by a void where its lower wall remains undamaged (central portion of the micrograph). Hence, voids are found to influence crack path and play an important role in deciding the mechanical properties at high strain rates.

5 CONCLUSIONS

Split Hopkinson Pressure Bar (SHPB) is found to be an effective instrument for testing the high strain rate properties of both fiber reinforced and particulate reinforced polymer matrix composites. Experimental characterization is found useful in order to verify scientific requirements of testing technique. Both graphite/epoxy laminates and syntactic foams are found to be highly strain rate sensitive. Both mechanical properties and failure modes are found to vary significantly in high strain rate testing as compared to quasi-static testing. In both of these composites, the viscoelastic nature of the polymer matrix itself is responsible for this phenomenon in addition to the time dependent nature of accumulating damage. Also some specific conclusions drawn from the high strain rate testing of these materials are the following.

Graphite/epoxy composites:

- The graphite/epoxy symmetric balanced angle ply laminates are found to be highly strain rate sensitive in a manner similar to unidirectional laminates of the same material. Continuous increase in maximum axial stress and strain has been observed with increasing strain rate for the fiber orientations examined.
- The stress remains constant with further increase in strain rate after achieving a certain maximum value of ultimate stress.
- Contrary to the behavior of the maximum stress value, the ultimate strain value increases continuously with increasing strain rate.
- The strain rate sensitivity of balanced angle-ply composite materials is observed to be strongly dependent on the fiber orientation. Even though fibers are strain rate insensitive, the strain rate effect on the ultimate stress and ultimate strain values gets more pronounced with decreasing fiber angle. This could be explained by the following

hypotheses, that is, the mode of failure of fiber reinforced composite materials is the determining factor of the strain rate sensitivity magnitude.

- A relatively smooth decrease in maximum stress and strain values with increase in fiber orientation angle has been obtained. This is contrary to the observations made for off-axis unidirectional fiber laminates, which shows sudden decrease in stress and strain for 60^{o} off-axis fiber orientation due to shear failure caused by the in-plane shear stresses. This mode of failure is avoided due to the inherent behavior of balanced angle ply laminates.
- The modulus values generally show an appreciable increase in dynamic testing as compared to the static ones.
- Delamination and matrix cracking are found to be the dominant modes of failure for dynamically tested specimens.

Syntactic foams:

- Almost twofold increase in the maximum stress is seen for the samples tested at the strain rate of about $1700s^{-1}$ as compared to their quasi-static values. The strain rate sensitivity of maximum stress is found to vary with density of the foam and the strain rate range.
- Strain at maximum stress is found to be almost constant for foams containing all types of cenospheres. The failure strain values are observed to increase with increasing cenosphere internal radius. Strain rate sensitivity of failure strain for syntactic foam depends on the density of the foam and the applied strain rate.
- Continuous increase in modulus unlike metallic foams is seen with increasing strain rate due to viscoelastic nature of polymeric matrix.
- Increase in energy absorbed at a particular strain value is observed for all type of foams as a result of increased strain rate.

- Failure initiated by shear at one of the specimen ends found to propagate along the length of the specimen creating flat fracture surfaces showing its ‘perfect brittle-like’ character. The crack doesn’t deviate its path to avoid the harder cenospheres until it causes the ultimate fracture of the specimen unlike the one observed under low strain rate conditions.

REFERENCES

1. Barr A. and Bouamrata A., Composites 19, (1988) pp. 453.

2. Bouhili R., Hubert P. and Gauvin R., Composites 22, (1991) pp. 39.

3. Daniel I. M. and LaBedz R. H., Compression Testing of Homogeneous Materials and Composites, ASTM STP 808, R. Papirno (eds.), American Society for Testing and Materials, Philaelphia, (1983), pp. 121.

4. Kolsky H. Stress Waves in Solids, Clarendon Press, Oxford (1953).

5. Staab G. H. and Gilat A., Journal of Composite Materials, Vol. 29, No. 10 (1995) pp. 1308.

6. Gilat A, Goldberg R K and Roberts G D., Com. Sc Tech. 62 (2002) pp. 1469.

7. LaLaillade J. L., Delaet M. and Collombet F., Proceedings, 9th ICCM, Madrid, Spain, Vol. V, (1993) pp. 358.

8. Gupta N., Kishore, Woldesenbet E. and Sankaran S., J. Mater. Sci. 36, 18 (2001) pp. 4485.

9. Gupta N., Woldesenbet E. and Kishore, J. Mater. Sci. 37, 15 (2002) 3199.

10. Karthikeyan C. S., Sankaran S., Jagdish Kumar M. N. and Kishore, J. Appl. Poly. Sci. 81 (2001) pp. 405.

11. Rizzi E., Papa E. and Corigliano A., Int. J. Solids Struct. 37 (2000) pp. 5773.

12. . D'almeida J. R. M, Compos. Sci. Technol. 59 (1999) pp. 2087.

13. Bunn P. and Mottram R. T., Composites 24, 7 (1993) pp. 565.

14. Progelhof R. C., in Proceedings of Instrumented Impact Testing of Plastics and Composite Materials, Houston, March 1986, (ASTM) pp. 105.

15. Sounik D. F., Gansen P., Clemons J. L., and Liddle J. W., Journal of Materials and Manufacturing. 106 (5) (1997) pp. 211.

16. Hall W., Guden M., and Yu C. J., Scripta Mater. 34 (2000) pp. 515.

17. Dannemann K. A., and Lankford J., Materials Science and Engineering. A293 (2000) pp. 157.

18. Mukai T., Kanahashi H., Miyoshi T., Mabuchi M., Nieh, and Higashi K., Scripta Materialia, 40 (8) (1999) pp. 921.

19. Deshpande V. S., Fleck N. A., International Journal of Impact Engineering. 24 (3) (2000) pp. 277.

20. Chen W., Lu F.and Winfree N., in Experimental Mechanics. 2002, 42(1), pp. 62.

21. Rinde J. A., and Hoge K. G., Journal of Applied Polymer Science. 1971 (15) pp. 1377.

22. BakerW. E., Togami T. C., and Weider J. C., Int. J. Impact Engng.21(3) (1998) pp. 149.

23. Zhao H., and Gary G., Int. J. Impact Engng. 21(10) (1998) pp. 827.

24. V. P. W. Shim, C. T. Lim, and K. J. Foo, Int. J. Impact Engng. 25 (2001) pp.15.

25. Venkatraman, S.; Kishore, Journal of reinforced plastics and composites 16(7) (1997) 618.

26. Han F., Zhu Z., and Gao J., Metallurgical and Materials Transactions A. 29A (1998) pp. 2497.

27. Shim V. P. W., Tu Z. H., and Lim C. T., Int. J. Impact Engng. 24 (2000) pp. 703.

28. Vinson J. R. and Woldesenbet E., J Compos Mater. 35(06) 2001 pp. 509.

29. Kaiser M A, Wicks A, Wilson L, Saunders W. Advancement in the Split Hopkinson Bar Test. Thesis Submitted to Virginia Polytechnic Institute and State University, Blacksburg, Virginia (1998); pp. 1-84.

30. Gama B. A., Gillespie J. W., Hassan M., Raines R. P., Haque A., Jeelani S, Bogetti T A, and Fink B K., J Compos Mater;35(13), (2001) pp. 1201.

31. Lindholm U. S., J. Mech. Phys. Solids 12, (1964) pp. 317.

32. Corigliano A, Rizzi E, and Papa E, Comp Sci Tech 60 (2000) pp. 2169.

33. T. Yoneyama, Doi H., E. Kobayashi, and H. Hamanaka, J. Mater. Sci. 11 (2000) pp. 333.

34. Hsio H M, Daniel I. M. and Cordes R D., J Compos Mater 33(17), (1999) pp. 1620.

35. Woldesenbet E. and Vinson J. R., AIAA Journal 37(9), (1999), pp.1102.

36. Eskandari H and Nemes J. A., J Compos Mater 34(4), (2000) pp. 260.

37. Agarwal B D and Broutman L J. Analysis and Performance of Fiber Composites. John Wiley and Sons, Inc. New York (1990).

VITA

Amol Jadhav was born on July 5, 1978 in India. He received his Bachelor of Science degree in metallurgical engineering in 1999 from University of Pune, India. After graduation he was employed as a Graduate Engineer in Elpro International Ltd. (Associated with G.E.).

In August 2001 he came to the United States and joined Louisiana State University to pursue a Master of Science degree in engineering. There he studied materials science under the Mechanical Engineering Department. He successfully defended his thesis work on June 30, 2003, and expects to receive a degree of Master of Science in Engineering Science in August 2003. During his master's study, he served as a research assistant and was also a teaching assistant for courses such as engineering materials laboratory and materials engineering. He is also an active member of the ASME.